Sodium incorporation into inorganic CaCO$_3$ and implications for biogenic carbonates

L.S. Devriendt [a,b,1,*], E.M. Mezger [a,1], E.K. Olsen [b], J.M. Watkins [b], K. Kaczmarek [c],
G. Nehrke [c], L.J. de Nooijer [a], G.-J. Reichart [a,d]

[a] Department of Ocean Systems, Royal Netherlands Institute for Sea Research (NIOZ), and Utrecht University, Texel, The Netherlands
[b] Department of Earth Sciences, University of Oregon, Eugene, OR, United States
[c] Alfred-Wegener-Institut Helmholtz-Zentrum für Polar- und Meeresforschung, Am Handelshafen 12, 27570 Bremerhaven, Germany
[d] Department of Earth Sciences, Faculty of Geosciences, Utrecht University, Heidelberglaan 2, 3584 CS Utrecht, The Netherlands

Abstract

The sodium content of biogenic carbonates shows potential as a palaeoceanographic proxy for salinity and/or calcium concentration but the incorporation of Na$^+$ into inorganic and biogenic calcite is poorly understood. Taxonomic and conspecific variations in the sensitivity of carbonate Na/Ca to seawater Na$^+$/Ca^{2+} and salinity point to a biological influence on Na$^+$ partitioning and/or covariations with other environmental parameters. One major unknown of the biological control during calcification is the rate of mineral precipitation, which has a strong control on trace-element partitioning in inorganic carbonate systems. We conducted inorganic CaCO$_3$ precipitation experiments where the effect of solution composition and crystal growth rate on Na$^+$ uptake by carbonate crystals are independently assessed. Calcite crystals were precipitated at rates varying from $10^{-6.5}$ to $10^{-4.5}$ mol/m^2/s, while faster growth rate than $10^{-4.5}$ mol/m^2/s resulted in the coprecipitation of aragonite and vaterite. For a given crystal growth rate, calcite Na/Ca increases by 0.22% per % increase in solution (Na$^+$)^2/Ca^{2+} activity ratio. However, calcite Na/Ca increases up to fivefold per order of magnitude increase in crystal growth rate, suggesting crystal growth rate and precursor phases are likely dominant controls on marine carbonate Na/Ca. We use these results in the framework of the DePaolo (2011) model for trace element uptake by calcite to assess the origin of variable (Na/Ca)$_{foraminifer}$ sensitivities to [Ca^{2+}]$_{seawater}$ and salinity. Last, maximum mineral growth rates are estimated for a range of marine carbonates based on known carbonate Na/Ca and the (Na$^+$)^2/Ca^{2+} activity ratio of seawater. Estimated rates vary from $10^{-5.6}$ (planktic foraminifers) to above 10^{-4} (sea urchins) mol/m^2/s. Such high mineral growth rates imply high degrees of oversaturation with respect to calcite (10 to >100), supporting the idea that elemental partitioning and isotopic fractionation recorded in marine biogenic carbonates are controlled by kinetic rather than equilibrium exchanges.
© 2021 The Author(s). Published by Elsevier Ltd. This is an open access article under the CC BY license (http://creativecommons.org/licenses/by/4.0/).

Keywords: Na/Ca; Sodium; Calcite; CaCO$_3$; Crystal growth rate; Salinity; Calcium concentration; Foraminifer; Marine carbonates; Mineral growth rate

1. INTRODUCTION

1.1. General background

The trace-element compositions of inorganic and biogenic CaCO$_3$ are commonly used as proxies to reconstruct past environments. This approach uses the dependency of

---

* Corresponding author at: Department of Ocean System Sciences, Royal Netherlands Institute for Sea Research, and Utrecht University, Texel, Netherlands.
E-mail address: laurent.devriendt@gmail.com (L.S. Devriendt).
[1] These two authors contributed equally.

element incorporation into $CaCO_3$ on environmental parameters (e.g. using the effect of temperature on Mg/Ca: Nürnberg et al., 1996; Lea et al., 1999; Elderfield and Ganssen, 2000). Foraminiferal calcite Na/Ca has been proposed as a proxy for salinity (Wit et al., 2013; Allen et al., 2016; Mezger et al., 2016, 2018, 2019; Bertlich et al., 2018; Geerken et al., 2018) and seawater Ca^{2+} concentration (Hauzer et al., 2018; Zhou et al., 2021) based on empirical calibrations from culture experiments and from field studies.

However, the fundamental variables behind the 'salinity' and 'Ca^{2+} concentration' effects have yet to be validated and the interplay of multiple driving variables could potentially complicate applications of the calcite Na/Ca proxy. Two significantly distinct models of Na^+ incorporation in calcite have been suggested based on inorganic calcite growth experiments: (1) crystal lattice incorporation of Na^+ where two Na^+ substitute for one Ca^{2+} and calcite Na/Ca is a function of the solution $(Na^+)^2/Ca^{2+}$ activity ratio (White, 1977, 1978) and (2) interstitial occupation of Na^+ where calcite Na/Ca depends on the solution Na^+ concentration or activity and number of lattice defects (Kitano et al., 1975; Ishikawa and Ichikuni, 1984; Busenberg and Plummer, 1985; Okumura and Kitano, 1986). In addition, calcite Na/Ca has been shown to significantly increase with increasing crystal growth rate and the solution SO_4^{2-} concentration (Busenberg and Plummer, 1985) as well as with the solution citrate concentration (White, 1978). The effects of individual parameters on Na^+ uptake by calcite have not yet been integrated into a predictive model of calcite Na/Ca due to the absence of data on crystal growth rate (Kitano et al., 1975; White, 1978; Ishikawa and Ichikuni, 1984) and/or correlations between multiple parameters affecting Na^+ partitioning. For example, Busenberg and Plummer (1985) reported an increase in Na^+ incorporation into calcite with increasing crystal growth rate but variable concentrations of SO_4^{2-} in solution (and in calcite) interfered with the solution-crystal Na^+ exchange and prevented a clear assessment of the impact of crystal growth rate on calcite Na/Ca.

With regards to biogenic $CaCO_3$, calcification commonly occurs in solutions with altered chemistries relative to the surrounding environment, contributing to elemental offsets between taxa that precipitated within the same environment (e.g. foraminifers: Erez, 2003; de Nooijer et al., 2014) and in heterogeneities within their shell walls (e.g. Spero et al., 2015; Branson et al., 2016; Fehrenbacher et al., 2017; Mezger et al., 2018, 2019; Bonnin et al., 2019; Geerken et al., 2019). For example, the precipitation of foraminifer tests involves selective ion transport (Bentov and Erez, 2006; Nehrke et al., 2013; de Nooijer et al., 2014), pH regulation (Bentov et al., 2009; de Nooijer et al., 2009a, 2009b; Toyofuku et al., 2017), transport of (modified) seawater to the site of calcification (vacuolization; Erez, 2003; Bentov and Erez, 2006), and the synthesis of organic molecules (e.g. Branson et al., 2016). The tests of marine calcifiers may therefore form under variable solution $[Na^+]$ and $[Ca^{2+}]$ distinct from those of seawater, as well as under highly variable calcite saturation states and crystal growth rates. Lastly, the formation of precursor

phases such as vaterite (e.g. Jacob et al., 2017) may have a significant effect on Na^+ partitioning. Investigating Na^+ partitioning over a wide range of ionic concentrations and calcite saturation state is therefore necessary to the development of models of Na^+ partitioning relevant to biogenic $CaCO_3$.

Here we aim to identify and quantify the primary factors controlling Na^+ incorporation into calcite over a wide range of solution $[Na^+]$ (0.001–1.4 M), $[Ca^{2+}]$ (1.0–30 mM) and crystal growth rate ($10^{-6.5}$–$10^{-3.3}$ mol/m^2/s) without interferences from additional impurity ions (e.g. Mg^{2+}, SO_4^{2-}). Crystal growth rates are varied by changing the solution saturation state with respect to calcite (2–200) and the Ca^{2+}/CO_3^{2-} activity ratio (0.3–5000). Our experimental results are used to develop a numerical model relating calcite Na/Ca to the solution $(Na^+)^2/Ca^{2+}$ activity ratio and crystal growth rate. The effect of SO_4^{2-} ions on Na^+ partitioning is also investigated by reassessing previous work in light of our new results. Implications for the use of biogenic carbonate Na/Ca as a salinity and Ca^{2+} concentration indicator are discussed and we provide first order approximations of crystal growth rates for a variety of marine calcifiers based on previously published biogenic calcite Na/Ca values.

1.2. Mechanism of Na^+ incorporation in $CaCO_3$

Past studies suggested an interstitial occupation of Na^+ in calcite and aragonite (Ishikawa and Ichikuni, 1984; Busenberg and Plummer, 1985; Okumura and Kitano, 1986), which involves the solution Na^+ concentration or activity as a main driver of carbonate Na/Ca. The Busenberg and Plummer (1985) model involves the substitution of two $CaCO_3$ groups by Na_2SO_4. However, synchrotron X-ray spectroscopy results from a range of calcite and aragonite samples indicate negligible presence of Na_2SO_4 (Yoshimura et al., 2017) despite the non-negligible presence of SO_4^{2-} in biogenic $CaCO_3$. The X-ray spectroscopy results show the presence of Na in calcite and aragonite is mainly in the form of Na_2CO_3. Yoshimura et al. (2017) suggest the incorporation of Na_2CO_3 into the $CaCO_3$ lattice is accommodated by a CO_3^{2-} vacancy (i.e., replacement of two $CaCO_3$ groups by one Na_2CO_3 group), similarly to the White (1977) model. This model can explain the presence of a significant amount of Na in $CaCO_3$ for carbonate minerals formed in solutions without the presence of additional impurity ions. According to this model of Na-incorporation, $CaCO_3$ growth in simple NaCl solutions can be viewed in terms of the following two reactions:

$$2Ca^{2+} + 2CO_3^{2-} \overset{K_1}{\rightleftharpoons} 2CaCO_3 \qquad (1)$$

$$2Na^+ + CO_3^{2-} \overset{K_2}{\rightleftharpoons} Na_2CO_3 \qquad (2)$$

With the equilibrium constants K_1 and K_2 expressed as follows:

$$K_1 = \frac{a^2_{CaCO_3}}{a^2_{Ca^{2+}} \cdot a^2_{CO_3^{2-}}} \qquad (3)$$

$$K_2 = \frac{a_{Na_2CO_3}}{a_{Na^+}^2 \cdot a_{CO_3^{2-}}} \tag{4}$$

where a_i is the free activity of the relevant ion or mineral phase. From (3) and (4), the equilibrium activities of $CaCO_3$ and Na_2CO_3 are obtained:

$$a_{CaCO_3} = \sqrt{K_1}(a_{Ca^{2+}} \cdot a_{CO_3^{2-}}) \tag{5}$$

$$a_{Na_2CO_3} = \sqrt{K_2}\left(a_{Na^+}^2 \cdot a_{CO_3^{2-}}\right) \tag{6}$$

and from (5) and (6), the Na/Ca ratio of calcite near chemical equilibrium conditions is obtained:

$$\left(\frac{Na}{Ca}\right)_{calcite} = \frac{2a_{Na_2CO_3}}{a_{CaCO_3}} \tag{7}$$

$$\left(\frac{Na}{Ca}\right)_{calcite} = \frac{2K_2}{\sqrt{K_1}} \cdot \frac{a_{Na^{2+}}^2}{a_{Ca^{2+}}} \tag{8}$$

This model involves a dependency of calcite Na/Ca on the solution $(Na^+)^2/Ca^{2+}$ activity ratio. Hence, calcite Na/Ca is expected to be negatively correlated with the solution Ca^{2+} concentration and, where the solution Na^+/Ca^{2+} concentration ratio remains constant, positively correlated with salinity.

2. METHODOLOGY

Three sets of inorganic $CaCO_3$ growth experiments were conducted to investigate the effect of solution $(Na^+)^2/Ca^{2+}$ activity ratio $(a_{Na^+}^2/a_{Ca^{2+}})$, Na^+ activity (a_{Na^+}), crystal growth rate (R_c), and $CaCO_3$ polymorphism on calcium carbonate Na/Ca $((Na/Ca)_c)$. Calcite growth experiments lasting several days $(LogR_c < -6$ mol/m²/s, from here on called 'slow growth') were carried with a CO_2 bubbling system at the University of Oregon (Section 2.1, Fig. 1a, b and c; Watkins et al., 2013) while experiments with higher crystal growth rates $(LogR_c = -6.0$ to -3.3 mol/m²/s; from here on called 'fast growth') were carried out using a Metrohm chemostat at the Royal Netherlands Institute for Sea Research (Section 2.2 and 2.3, Fig. 1d, e and f; Kaczmarek et al., 2016). The use of two experimental setups was necessary to achieve a wide range of crystal growth rates $(10^{-6.5}–10^{-3.3}$ mol/m²/s) and solution $a_{Na^+}^2/a_{Ca^{2+}}$ (~10^{-4} to 650). Prior to each experiment, plastic and glassware were acid-washed, rinsed with deionised water (18.2 MΩ) three times and all solutions were left to equilibrate with the laboratory's controlled temperature for a minimum of 12 hours (25.0 ± 0.5 °C). The solution ionic strengths and ionic free activities were calculated using the PHREEQc R-package (version 3.6.0, Charlton and Parkhurst, 2011) with the Pitzer database. The use of PHREEQc databases other than Pitzer resulted in erroneous ionic activity coefficients at ionic strength higher than 0.5 (Fig. A1) and are therefore not recommended for solutions with salinities close to or above the ionic strength of seawater. Calcite saturation states $(\Omega_{calcite} = a_{Ca^{2+}} \times a_{CO_3^{2-}}/K_{sp})$ were calculated from the activities of free Ca^+ and CO_3^{2-} and the activity-based solubility product for calcite at 25 °C $(K_{sp} = 10^{-8.42},$ Jacobson and Langmuir, 1974).

2.1. Experiment group 1: slow R_c with variable $[Na^+]_w$ (CO_2 bubbling)

Calcite crystals were precipitated slowly $(LogR_c = -6.5$ to -6.1 mol/m²/s under different solution Na^+ concentrations $([Na^+]_w = 1.4$ mM–1.4 M) but identical Ca^{2+} concentrations $([Ca^{2+}]_w = 30$ mM) to investigate the effect of $a_{Na^+}^2/a_{Ca^{2+}}$ on $(Na/Ca)_c$. Crystal growth rates (R_c) were very similar within this set of experiments because solutions with higher ionic strength had higher steady state dissolved inorganic carbon concentrations $([DIC]_w$; i.e. the activity product of CO_3^{2-} and Ca^{2+} remained similar among these experiments). These experiments were conducted following a similar protocol as described in Watkins et al. (2013) whereby CO_2 gas (200 ppm) was bubbled throughout experiment durations of 41 to 93 hours into a stirred solution (1.7 L), containing 30 mM $CaCl_2 \bullet 2H_2O$, 5 mM NH_4-Cl and 0 to 1.37 M NaCl (Fig. 1a). The pH was monitored and controlled at 8.30 ± 0.07 using an autotitrator (Jensen systems) with 1 M NaOH solution, combined with Titronic universal burettes and an NBS-calibrated BlueLine pH combination electrode (Schott Instruments). The small addition of NaOH (2.3–5.7 mM) and decrease of $[Ca^{2+}]_w$ (~8%) during the course of the experiments were taken into account for calculating the average $a_{Na^+}^2/a_{Ca^{2+}}$ values of each experiment. Calcite nucleation and precipitation occurred after $\Omega_{calcite}$ reached 7.5 ± 1.5. Following nucleation, $\Omega_{calcite}$ decreased to 3.3 ± 1.2 until the system reached steady state conditions (Fig. 1b). Estimation of $\Omega_{calcite}$ during the course of an experiment was achieved by regular solution sampling (3.5 mL) and subsequent $[DIC]_w$ analyses.

For $[DIC]_w$ analyses, 3.5 mL of solution reacted with 0.1 mL of 85% orthophosphoric acid in He-flushed exetainers. After equilibrating for 4 hours, the gas headspace was analysed by continuous-flow mass spectrometry on a GasBench-DeltaV system. A known concentration of in-house $NaHCO_3$ standard was analysed with the samples, from which a calibration curve was determined.

At the end of each experiment, the solution and any suspended crystals were discarded. The remaining crystals (Fig. 1c) attached to the bottom and sides of the beaker were rinsed at least three times with de-ionised water, air-dried, and then gently detached from the walls of the beaker using a plastic spatula. Average R_c (mol/m²/s) were determined from the decrease in $[Ca^{2+}]_w$ (as estimated from the difference between the NaOH added and the final solution total alkalinity) and the estimated average surface area of calcite crystals (Tang et al., 2008):

$$R_c = \frac{0.5(NaOH_f - TA_f) \cdot V}{t \cdot SA^*}, \tag{9}$$

where the 0.5 factor accounts for Ca^{2+} having 2 equivalents per mole, $NaOH_f$ is the total NaOH (Eq/L) titrated into solution at the end of the experiment, TA_f is the solution total alkalinity (Eq/L) at the end of the experiment as measured by Gran titration, V is the solution volume (L), t is the duration of calcite precipitation (s), and SA^* is the estimated average geometric surface area during an experiment:
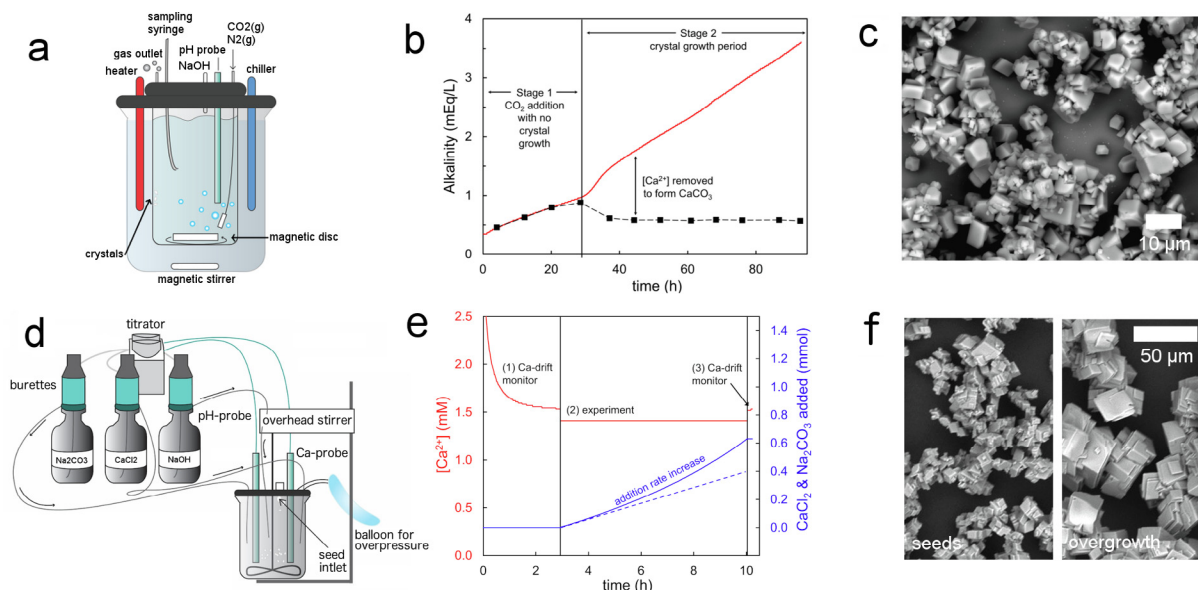
Fig. 1. Experimental setups, behaviours and recovered calcite samples for the $CaCO_3$ growth experiments performed in this study. (a) CO_2 bubbling system (similar to Watkins et al., 2013) used for slow calcite growth experiments lasting several days. (b) Example of an experimental run (S13) using the CO_2 bubbling system. The alkalinity increase due to NaOH addition (red curve) is offset by alkalinity removal to $CaCO_3$, leading to a total alkalinity (black squares) that is nearly constant during the crystal growth period. (c) Calcite crystals recovered at the end of an experiment carried out with the CO_2 bubbling system. (d) Chemostat system (similar to Kaczmarek et al., 2016) used in a temperature-controlled room (25 ± 0.5 °C) for experiments lasting less than 24 h. (e) Example of an experimental run (40_2) using the chemostat system. Potential drift of the calcium electrode reading was monitored before and after each experimental run (step 1 and 3). The small increase in the rate of $CaCl_2$ and Na_2CO_3 additions during the course of an experiment (step 2) reflects an increase in the reactive surface area. (f) Calcite seed crystals and overgrown calcite crystals recovered at the end of an experiment carried out with the chemostat system.

$$SA^* = \frac{Sp \times m_{CaCO_3}}{2}, \qquad (10)$$

where Sp is the specific surface area of calcite crystals at the end of an experiment (0.3 ± 0.1 m^2/g for an average particle size of ~ 10 μm determined from SEM images, Figs. 1c and A1, Tang et al., 2008), m_{CaCO_3} is the total mass (g) of calcite precipitated and the denominator value of 2 applies to obtain the average geometric surface area during an experiment knowing that initial SA^* is 0 m^2/g. Reported average R_c and $\Omega_{calcite}$ values for each experiment are representative of steady state growth conditions rather than conditions during the initial and brief nucleation stage (see the 'Stage 2' period of near-constant rate of $CaCO_3$ formation under near-constant alkalinity on Fig. 1b).

2.2. Experiment group 2: various R_c with constant $[Na]_w$ (chemostat)

Calcium carbonate crystals were precipitated for 2–24 hours using a modified version of the protocol described in Kaczmarek et al. (2016). This experimental setup consists of a titrator (Stat 902 Titrando, Metrohm, 2.902.0010), three burettes (800 Dosino, Metrohm, 2.800.0010), a combined polymer calcium electrode (6.0510.100) and a pH electrode (6.0262.100; Fig. 1d). All devices are connected to the titrator and controlled via the Tiamo 2.5 software. This equipment allows for keeping the solution pH, $[Ca^{2+}]_w$ and $[CO_3^{2-}]_w$ constant during the course of an

experiment by additions of burette solutions, which compensate for Ca^{2+} and CO_3^{2-} loss by $CaCO_3$ precipitation. It was found that the calcium-electrode reading drifted significantly (>7 mV, equivalent to > 50% change in $[Ca^{2+}]_w$) during the first 1–2 hours of measurement. Such a large drift in the signal of the calcium electrode was most likely caused by the high ionic strengths of the solution used in this study since stable readings were obtained in dilute solutions (Kaczmarek et al., 2016). To minimize the drift of the calcium reading, the electrode was conditioned for ~ 2–3 hours before the start of each experiment (Fig. 1e) using a solution with $[Ca^{2+}]_w$ and $[Na^+]_w$ identical to that of the growth solution but without added DIC to keep the solution undersaturated with respect to calcite. Although a conditioning step greatly reduced the drift of the calcium electrode reading for experiments lasting less than ~ 24 h, it did not permit us to conduct stable experiments lasting several days. Hence, slow growth experiments were conducted with a different experimental setup (see previous Section 2.1).

Following stabilization of the calcium electrode signal, 100 mL of $CaCl_2$ solution was mixed with 100 mL of Na_2CO_3 solution to form a 200 mL oversaturated solution ($\Omega_{calcite} \sim 2$–190, $[Ca^{2+}]_w = [DIC]_w = 0.7$–5 mM, pH = 9.90 ± 0.15; Log$R_c = -6.0$ to -3.5 mol/m^2/s) and a constant $[Na^+]_w$ of 0.47 M to evaluate the effect of R_c and $a^2_{Na^+}/a_{Ca^{2+}}$ on $(Na/Ca)_c$ at seawater $[Na^+]_w$. The oversaturated solution was kept in an air-tight glass beaker connected to the

3 burettes with matching NaCl concentrations (e.g. burette 1: 14 mM CaCl$_2$, burette 2: 14 mM Na$_2$CO$_3$, burette 3: 50 mM NaOH, Fig. 1d). Shortly after solution mixing, calcite seeds (Alfa Aesar, 10–32 μm diameter, (Na/Ca)$_c$ < 0.01 mmol/mol) were immersed in 1–2 mL of the oversaturated solution, then immediately transferred to the 200 mL oversaturated solution to initiate calcite growth. CaCl$_2$ and Na$_2$CO$_3$ addition rates typically increased during the course of an experiment (Fig. 1e), due to the increase in reactive surface area of the growing crystals. At the end of each experiment, the solution and detached crystals (Fig. 1f) were immediately vacuumed-filtered (0.45 μm), then rinsed three times with de-ionised water. Potential drift of the calcium electrode reading during the course of an experiment was estimated by remeasuring the conditioning solution (matrix-matched but undersaturated) with the calcium electrode at the end of each experiment. Typical drift of the calcium electrode reading was 0–10% and remained below 20% with respect to the initial growth solution [Ca^{2+}]$_w$. The amount of CaCO$_3$ accumulated during each experiment was inferred from the total amount of CaCl$_2$ added and accounts for any small decrease in [Ca^{2+}]$_w$ during the course of an experiment caused by a drift of the calcium electrode reading ($n_{CaCO_3} = n_{CaCl_2\_added} + n_{Ca\_initial} - n_{Ca\_final}$). The mean R_c value for each experiment was calculated from:

$$Rc = \frac{n_{CaCO_3}}{SA \cdot t}, \tag{11}$$

where t is the duration of calcite precipitation in seconds and SA is the average geometric surface area:

$$SA = 0.5(\eta + 1) \cdot Sp_{seeds} \cdot m_{seeds} \tag{12}$$

where Sp_{seeds} is the specific surface area of calcite seeds (0.35 ± 0.02 m^2/g, determined with a TriStar 3000 Brunauer-Emmett-Teller analyser using N$_2$, Utrecht University), m_{seeds} is the mass of calcite seeds added (∼5 mg) and η is the relative increase in the reactive surface area between the start and end of an experiment (determined from the increase in CaCl$_2$ addition rates, Fig. 1e). The 0.5 factor applies to obtain the average geometric surface area during an experiment.

Experiments with $\Omega_{calcite}$ values above 18 ($n = 5$, CV and CAV samples) were conducted without the addition of calcite seeds due to the coprecipitation of aragonite and vaterite (Fig. A2). The R_c values for unseeded experiments were estimated from the empirical relationship between total crystal surface area and total crystal weight obtained from the seeded experiments ($r^2 = 0.85$, p-value <0.01; Fig. A3). The latter method is justified by the fact that the average diameter of individual crystals was similar for seeded and unseeded experiments (i.e. 20–40 μm, Fig. A2). We note however that the estimated R_c values for the unseeded experiments are less precise compared to the seeded experiments due to coprecipitation of aragonite and vaterite and the absence of accurate constraints on the specific surface area of these crystals. To account for this, uncertainties of ±50% of the value of estimated R_c values were applied for the unseeded experiments but this does not compromise the overall patterns and conclusions reached in this study.

2.3. Experiment group 3: fast R_c with variable [Na$^+$]$_w$ (chemostat)

Calcite crystals were precipitated following the same protocol described in Section 2.2 but under different [Na$^+$]$_w$ (0.4 to 0.6 M) and very similar $\Omega_{calcite}$ of 11.5 ± 0.5 ([Ca^{2+}]$_w$ = [DIC]$_w$ = 1.3–1.5 mM) to investigate the effect of $a^2_{Na^+}/a_{Ca^{2+}}$ (250 to 500) on (Na/Ca)$_c$ in conditions far from chemical equilibrium and for solutions with [Na$^+$]$_w$ similar to the range of variability of natural seawater. The pH of these experiments was 10.0 ± 0.3. This resulted in similar crystal growth rates for all experiments ranging from 10$^{-5.3}$ to 10$^{-4.9}$ mol/m^2/s. Scanning electron microphotographs of the CaCO$_3$ samples (Fig. A2) show all samples are made of 100% calcite crystals of similar size, suggesting spontaneous nucleation did not occur or was insignificant relative to the accumulated calcite on seed material.

2.4. Cleaning of CaCO$_3$ samples and trace-element analysis

Following drying and weighing, the CaCO$_3$ samples were transferred to 0.2 mL Eppendorf vials, sonicated in deionised water for two minutes, centrifuged for 60 seconds at 2000 rpm after which the supernatant was removed. This cleaning procedure was repeated twice and was necessary to remove NaCl from the CaCO$_3$ samples (Fig. A4). Repeating the cleaning step up to five times for a sample did not improve the reproducibility of results and did not reduce the (Na/Ca)$_c$ ratios further (i.e. no indication of Na$^+$ leaching). A similar cleaning procedure but using Milli-Q saturated with respect to calcite instead of pure Milli-Q also resulted in very similar (Na/Ca)$_c$ ratios (Fig. A4), further confirming the cleaning procedure with pure Milli-Q is adequate and does not lead to preferential Na$^+$ leaching from the calcite crystals. Following cleaning and drying, the samples were dissolved in 0.1 M ultrapure HNO$_3$. The elemental composition of the CaCO$_3$ samples was measured on a Thermo Fisher Scientific iCAP-Q-ICP-MS at the Royal Netherlands Institute for Sea Research (Texel). The isotopes of ^{23}Na, ^{43}Ca and ^{44}Ca were measured in a cycle of 1.5 minutes. Samples were measured against 4 ratio calibration standards with a similar matrix, with a drift standard measured every third sample and converting isotope counts into elemental ratios. The monitor standards JCt-1 and NFHS-1 (Okai et al., 2002) were included for quality control. Elemental values were drift-corrected, even though drift was low (~1%). Accuracy based on the two quality control standards was 99 ± 2%. All reported (Na/Ca)$_c$ ratios were corrected for the contribution of calcite seeds (if any) based on the estimated amount of total CaCO$_3$ precipitated during each experiment (Sections 2.2).

2.5. XRD analysis

Samples for XRD were crushed to a fine powder under ethanol with a mortar and pestle. XRD samples were measured on a Bruker D8 Discover at Utrecht University, and scanned at 2° per minute for a 2θ range of 4-70°. The percent calcite/aragonite/vaterite in each sample was estimated

using TOPAS version 4.2 software (Rietveld refinement method) for analysing diffraction peaks.

3. RESULTS

A summary of results from all the experiments carried out in this study is presented in Table 1. For a more complete description of the experimental conditions and results, the reader is referred to the electronic database (Table A1).

3.1. Experiment group 1: slow R_c with variable $[Na^+]_w$ (CO_2 bubbling)

Calcite crystals precipitated slowly ($\log R_c = -6.5$ to -6.1 mol/m^2/s) with the CO_2 bubbling system have $(Na/Ca)_c$ spanning 0.13–1.55 mmol/mol over the 10^{-4}–125 range in $a_{Na^+}^2/a_{Ca^{2+}}$ (Fig. 2a; $[Na^+]_w = 0.001$–1.4 M, $[Ca^{2+}]_w = 30$ mM, pH = 8.3). The relationship between $(Na/Ca)_c$ and $a_{Na^+}^2/a_{Ca^{2+}}$ is not linear and is well-described by a power function ($r^2 = 0.96$):

Fig. 2. Sodium content of inorganic calcite as function of the solution $(Na^+)^2/Ca^{2+}$ activity ratios ($a_{Na^+}^2/a_{Ca^{2+}}$) for slow growth experiments (group 1, CO_2 bubbling system). (a) Calcite Na/Ca ($(Na/Ca)_c$) vs $a_{Na^+}^2/a_{Ca^{2+}}$ and (b) solution-calcite Na^+ partitioning (D_{Na}) vs $a_{Na^+}^2/a_{Ca^{2+}}$. These experiments were caried under very similar solution $[Ca^{2+}]$ (~30 mM) but different $[Na^+]$ (~10^{-3} to 1.4 M). The within-sample variability in $(Na/Ca)_c$ and D_{Na} was assessed for experiment S3 (± 2 RSD = 12.8%, $n = 11$) and is represented by the error bars in both panels. The calcite saturation state and mineral growth rate of these experiments remained within relatively small ranges (2.2 $<$ $\Omega_{calcite}$ $<$ 4.2; -6.5 $<$ $\log R_c$ $<$ -6.1 mol/m^2/s) except for one experiment (smaller circle: S15 excluded from the model fitting). Best fits with Eq. (13) (panel a) and Eq. (14) (panel b) are represented by the black curves.

$$(Na/Ca)_c = \Delta\left(a_{Na^+}^2/a_{Ca^{2+}}\right)^k \qquad (13)$$

where Δ and k are best-fit parameters ($\Delta = 4.2 \times 10^{-4}$ and $k = 0.22$ at $\log R_c \sim -6.3$ mol/m^2/s). The $(Na/Ca)_c$ values from this set of experiments is also well-fitted by a model using the explanatory variables a_{Na^+} (not shown) instead of $a_{Na^+}^2/a_{Ca^{2+}}$ since the same $[Ca^{2+}]_w$ was used for all experiments. However, results presented in Section 3.2 suggest $(Na/Ca)_c$ is controlled by $a_{Na^+}^2/a_{Ca^{2+}}$ (White, 1977, 1978) rather than a_{Na^+} (Busenberg and Plummer, 1985).

Small variations in crystal growth rate between these experiments could not be evaluated accurately because of uncertainties in the reactive surface areas during each experiment (calcite seeds were not used for this set of experiments). Instead, the solution mean $\Omega_{calcite}$ (2.2–5.3, Table 1) was used as a proxy for relative difference in crystal growth rate since $\Omega_{calcite}$ values are strongly correlated with R_c over the entire dataset presented in this study (Fig. A5). For these experiments, no significant $\Omega_{calcite}$ effect on $(Na/Ca)_c$ was resolved (Fig. 2a), except perhaps for the comparatively high $(Na/Ca)_c$ of experiment S15 ($(Na/Ca)_c = 1.55$ mmol/mol, $\Omega_{calcite} = 5.3$), which may have been caused by the higher $\Omega_{calcite}$ in comparison to the other experiments. Experiment S15 was therefore excluded when fitting equation (13) to the data.

Measurements of 11 different aliquots taken from the same calcite sample (Fig. 2a, $a_{Na^+}^2/a_{Ca^{2+}} = 18.5$, sample S3) resulted in a relative standard deviation (RSD) in $(Na/Ca)_c$ of 6.4%, which is significantly higher than the analytical precision of 0.8% (1 RSD) but does not compromise the reported trends in this study. The cause of sample heterogeneity in $(Na/Ca)_c$ may be due to minor refractory NaCl fractions and/or small variations in R_c during the course of an experiment (cf. Section 3.2).

3.2. Experiment group 2: various R_c with constant $[Na]_w$ (chemostat)

Chemostat experiments conducted under a constant $[Na^+]_w$ of 0.47 M but with variable $[Ca^{2+}]_w$ and $[CO_3^{2-}]_w$ resulted in the precipitation of 100% calcite in solution with $\Omega_{calcite}$ values ranging from 2.5 to 18 ($\log R_c < -4.7$ mol/m^2/s) while higher $\Omega_{calcite}$ values resulted in the coprecipitation of aragonite and vaterite with calcite. A semi-quantitative XRD analysis (see Fig. A6 for typical XRD spectrums) carried out on these samples indicates the aragonite fraction represents ~ 40% of the sample masses ($n = 2$, Fig. A2, Table A2) while the vaterite fraction ranges from ~1% to 14% ($n = 5$, Fig. A2, Table A2). The polymorph fractions were also assessed based on the % surface occupied by each polymorph on SEM microphotographs (Fig. A2) and yielded results compatible with the XRD analyses (Table A2).

Crystal growth rates were significantly faster when using the chemostat than the CO_2 bubbling apparatus (Section 3.1) despite some experiments having similar solution $\Omega_{calcite}$ (Fig. A5). This can be attributed to differences in the solution $a_{Ca^{2+}}/a_{CO_3^{2-}}$ (0.6–3.3 vs. >3900; Nehrke et al., 2007).

Variations in $(Na/Ca)_c$ ratios for all the $CaCO_3$ samples range from 3.4 to 33.2 mmol/mol and are strongly corre-

Table 1
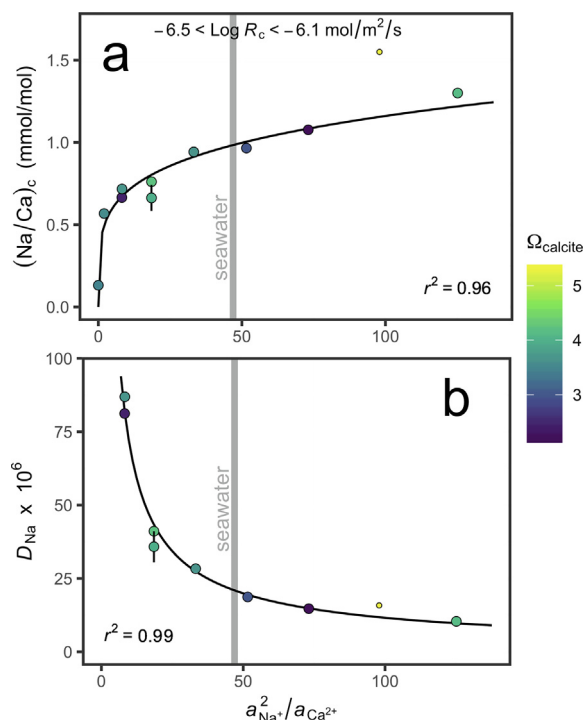Solution compositions, crystal growth rates, measured and modelled carbonate Na/Ca ratios for all experiments carried in this study.

Fig.	ID	Aparatus	Crystal[a]	pH$_{NBS}$ 25 °C	[Na$^+$] M	[Ca^{2+}] mM	[DIC] mM	$a_{Na^+}^2/a_{Ca^{2+}}$ [b] mol/mol	$\Omega_{calcite}$ [c]	$\log R_c$ mol/m^2/s	± mol/m^2/s	(Na/Ca)$_c$ mmol/mol	mod. (Na/Ca)$_c$
2, 3	S2	CO$_2$ bubbling	C	8.3	0.519	30.00	0.34	18.5	4.2	−6.26	0.12	0.76	1.08
2, 3	S3	CO$_2$ bubbling	C	8.3	0.519	30.00	0.32	18.5	4.0	−6.27	0.12	0.66	1.06
2	S5	CO$_2$ bubbling	C	8.3	0.349	30.00	0.18	8.2	2.5	−6.10	0.12	0.67	1.23
2	S7	CO$_2$ bubbling	C	8.3	0.178	30.00	0.22	2.0	3.6	−6.20	0.12	0.57	0.74
2	S8	CO$_2$ bubbling	C	8.3	0.001	30.00	0.15	9.7×10^{-5}	3.5	−6.27	0.12	0.13	0.07
2	S9	CO$_2$ bubbling	C	8.3	0.350	30.00	0.27	8.2	3.7	−6.24	0.12	0.72	0.95
2	S10	CO$_2$ bubbling	C	8.3	0.692	30.00	0.31	33.2	3.7	−6.34	0.12	0.94	1.05
2	S12	CO$_2$ bubbling	C	8.3	1.376	30.00	0.34	125.2	4.1	−6.17	0.12	1.30	1.94
2	S13	CO$_2$ bubbling	C	8.3	1.034	30.00	0.19	73.1	2.2	−6.54	0.12	1.08	0.87
2	S14	CO$_2$ bubbling	C	8.3	0.864	30.00	0.26	51.6	3.0	−6.30	0.12	0.97	1.27
2	S15	CO$_2$ bubbling	C	8.3	1.206	30.00	0.45	97.9	5.3	−6.31	0.12	1.55	1.43
3	35_1	Chemostat	C	9.9	0.469	1.00	1.00	440.0	6.0	−5.68	0.07	6.06	6.42
3	35_2	Chemostat	C	9.8	0.469	0.99	0.99	441.2	5.6	−5.52	0.06	7.62	8.34
3, 4	35_4	Chemostat	C	10.0	0.469	1.35	1.35	326.5	12.1	−5.25	0.03	12.18	11.56
3, 4	35_6	Chemostat	C	10.0	0.469	1.34	1.34	326.7	11.6	−5.11	0.05	12.59	13.68
3, 4	35_7	Chemostat	C	9.9	0.469	1.34	1.37	326.0	11.5	−5.17	0.04	13.11	12.80
3	35_8	Chemostat	C	10.0	0.469	1.65	1.65	266.7	17.9	−4.93	0.06	15.32	15.57
3	35_9	Chemostat	C	10.0	0.469	1.65	1.65	266.7	17.8	−4.80	0.06	16.39	17.26
3	35_10	Chemostat	C	9.8	0.469	0.69	0.69	635.9	2.6	−5.74	0.07	4.43	6.22
3	35_11	Chemostat	C	9.7	0.469	0.69	0.69	635.8	2.5	−6.01	0.07	3.45	3.79
3	35_12	Chemostat	CAV	10.2	0.469	2.61	2.59	169.4	49.3	−3.81	0.12	24.56	-
3	35_13	Chemostat	CAV	10.1	0.469	2.61	2.59	169.2	45.7	−4.11	0.12	21.98	-
3	35_14	Chemostat	CV	10.2	0.469	4.99	4.99	89.4	177.7	−3.70	0.12	29.53	-
3	35_15	Chemostat	CV	10.3	0.469	5.00	5.00	89.2	186.8	−3.51	0.12	33.20	-
3	35_16	Chemostat	CV	10.3	0.469	5.00	5.00	89.2	186.8	−3.39	0.12	29.49	-
3	35_17	Chemostat	C	10.2	0.469	0.68	2.69	650.7	13.6	−5.23	0.03	14.27	13.76
3	35_18	Chemostat	C	10.1	0.469	0.68	2.69	650.2	12.9	−5.13	0.04	15.76	15.47
4	30_1	Chemostat	C	10.0	0.403	1.28	1.27	251.8	11.6	−5.41	0.04	10.78	8.75
4	30_2	Chemostat	C	10.0	0.403	1.28	1.27	251.8	11.4	−5.16	0.04	12.12	12.10
4	30_4	Chemostat	C	10.0	0.403	1.27	1.27	253.8	11.5	−5.08	0.05	13.57	13.31
4	40_1	Chemostat	C	9.9	0.535	1.41	1.41	406.6	11.2	−5.12	0.05	13.90	14.09
4	40_2	Chemostat	C	9.9	0.535	1.41	1.41	406.5	10.7	−5.12	0.05	14.47	14.21
4	45_1	Chemostat	C	9.9	0.600	1.46	1.47	494.6	11.2	−5.05	0.05	15.64	15.85
4	45_2	Chemostat	C	9.9	0.600	1.47	1.47	491.1	11.1	−5.05	0.06	15.14	15.92

[a] Determined by XRD analysis and scanning electron microscopy, C: calcite, A: aragonite, V: vaterite.
[b] Ionic free activity coefficients computed using the PHREEQc R-package (Charlton and Parkhurst, 2011) with the *Pitzer* database.
[c] Computed with a calcite solubility product K_{sp} of $10^{-8.42}$ at 25 °C (Jacobson and Langmuir, 1974).

lated with crystal growth rates ($r^2 = 0.97$, p-value $<10^{-3}$, Fig. 3), while the solution $a_{Na^+}^2/a_{Ca^{2+}}$ (90 to 650), and crystal polymorphism seem to influence (Na/Ca)$_c$ to a lesser degree. Nevertheless, two pairs of experiments which resulted in 100% calcite (35_17 and 35_18 vs 35_4 and 35_7) and with almost identical a_{Na^+} (0.335 ± 0.001 M) and R_c (logR_c = −5.14 ± 0.07 mol/m^2/s) but distinct solution $a_{Na^+}^2/a_{Ca^{2+}}$ (325 vs 650) resulted in higher (Na/Ca)$_c$ values for the calcite grown in solution with the highest $a_{Na^+}^2/a_{Ca^{2+}}$ (14.3 and 15.8 vs 12.2 and 13.1 mmol/mol, Fig. 3). At near-constant R_c, a doubling in $a_{Na^+}^2/a_{Ca^{2+}}$ therefore resulted in a ~19.0% increase in (Na/Ca)$_c$, which is fairly consistent with the 16.4% increase in (Na/Ca)$_c$ predicted for a doubling in $a_{Na^+}^2/a_{Ca^{2+}}$ by Eq. (13). The highest (Na/Ca)$_c$ ratios were obtained for CaCO$_3$ samples that contained vaterite despite these samples having formed in solutions with comparatively low $a_{Na^+}^2/a_{Ca^{2+}}$, indicating enhanced incorporation of Na$^+$ in vaterite than in calcite.

3.3. Experiment group 3: fast R_c with variable [Na$^+$]$_w$ (chemostat)

Calcite crystals precipitated rapidly (logR_c = −5.3 to −4.9 mol/m^2/s) with the chemostat system but under variable [Na$^+$]$_w$ (0.4–0.6 M, range of natural seawater variation) have (Na/Ca)$_c$ ratios ranging from 10.8 to 15.6 mmol/mol. For these experiments, (Na/Ca)$_c$ is correlated with $a_{Na^+}^2/a_{Ca^{2+}}$ ($r^2 = 0.74$, p-value = 0.002, Fig. 4a) and with logR_c ($r^2 = 0.72$, p-value = 0.005, Fig. 4b), indicating that both solution chemistry and crystal growth rate affected (Na/Ca)$_c$ for this set of experiments. These results contrast with the slow growth experiments of Section 3.1, where the (Na/Ca)$_c$ results appear insensitive to small variations in solution $\Omega_{calcite}$ (and presumably R_c). Hence, where logR_c is close to −5.0 mol/m^2/s, small variations in crystal growth rate have a significant effect on Na$^+$ partitioning between calcite and solution.

3.4. Summary of results

Results from experiment 1 indicate that (Na/Ca)$_c$ is positively correlated with either $a_{Na^+}^2/a_{Ca^{2+}}$ or a_{Na^+} and small variations in R_c do not significantly affect (Na/Ca)$_c$ where R_c is on the order of 10^{-6} mol/m^2/s or lower.

Results from experiments 2 and 3 indicate (Na/Ca)$_c$ is strongly correlated with R_c where $R_c > 10^{-6}$ mol/m^2/s. Rapid precipitation of CaCO$_3$ with $R_c > 10^{-4.5}$ mol/m^2/s resulted in samples containing a small fraction of vaterite; these samples have the highest (Na/Ca)$_c$ reported in this study. Experiment 2 also indicates (Na/Ca)$_c$ increases with higher $a_{Na^+}^2/a_{Ca^{2+}}$ where a_{Na^+} and R_c are constant.

4. DISCUSSION

4.1. Controls on inorganic calcium carbonate Na/Ca

Variations in the Na/Ca ratio of inorganic calcium carbonate crystals have been related to the solution $a_{Na^+}^2/a_{Ca^{2+}}$
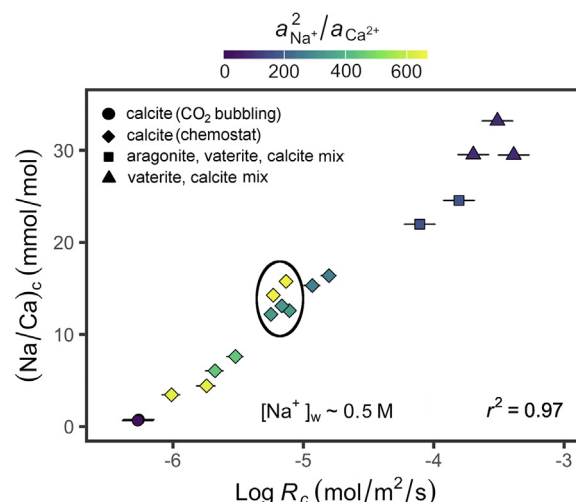

Fig. 3. Sodium content of calcium carbonate minerals (Na/Ca)$_c$ for fast growth experiments carried out with the chemostat system (group 2) under identical solution [Na$^+$] (0.47 M, seawater value) but different [Ca^{2+}] (~0.7–5.0 mM) and crystal growth rates ($10^{-6.0}$–$10^{-3.4}$ mol/m^2/s). Results from two calcite slow growth experiments carried under a solution [Na$^+$] of 0.52 M (circles: experiment group 1) are shown for comparison. Uncertainties in logR_c values (error bars) are mostly due to the uncertainty in the surface area of calcite crystals during the course of an experiment. Results from five calcite growth experiments performed under two different solution (Na$^+$)^2/Ca^{2+} activity ratios (~325 and ~650) but which resulted in similar crystal growth rates (LogR_c ~ −5.2 mol/m^2/s) are circled. These results indicate both crystal growth rate and the solution (Na$^+$)^2/Ca^{2+} activity ratio affect (Na/Ca)$_c$.

(White, 1977; 1978), a_{Na^+} (Ishikawa and Ichikuni, 1984; Busenberg and Plummer, 1985), the crystal growth rate (Busenberg and Plummer, 1985; Füger et al., 2019), the carbonate sulphate content (Kitano et al., 1975; Busenberg and Plummer, 1985) and the polymorph (Kitano et al., 1975). In the following sections, the effect of each of the above parameters on (Na/Ca)$_c$ is evaluated based on results of this study as well as from previous work.

4.1.1. Calcite-solution Na$^+$ partitioning

Early work showed Na$^+$ uptake in calcite and aragonite becomes significantly less sensitive to the solution [Na$^+$]$_w$ with increasing [Na$^+$]$_w$ (i.e. Freundlich isotherm behaviour; Kitano et al., 1975; Ishikawa and Ichikuni, 1984). These early results were interpreted as Na$^+$ occupying interstitial lattice positions, suggesting (Na/Ca)$_c$ should be controlled by a_{Na^+} (Kitano et al., 1975; Ishikawa and Ichikuni, 1984) rather than $a_{Na^+}^2/a_{Ca^{2+}}$ (as in White, 1977; 1978). However, covariations between a_{Na^+} and $a_{Na^+}^2/a_{Ca^{2+}}$ during the Kitano et al. (1975) and Ishikawa and Ichikuni (1984) experiments, along with the absence of information on crystal growth rates, did not allow them to assess the effects of a_{Na^+} and $a_{Na^+}^2/a_{Ca^{2+}}$ on (Na/Ca)$_c$ independently.

Results from experiment 2 suggest a $a_{Na^+}^2/a_{Ca^{2+}}$ control (rather than a_{Na^+}) on (Na/Ca)$_c$ since Na/Ca ratios are 19% higher for calcite formed with $a_{Na^+}^2/a_{Ca^{2+}}$ doubled
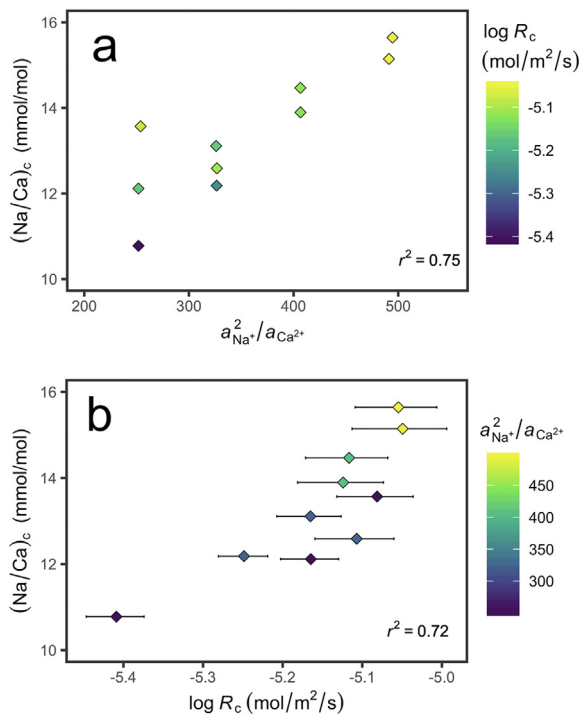
Fig. 4. Sodium content of calcite crystals $(Na/Ca)_c$ for fast growth experiments carried out with the chemostat system (group 3) under different solution $[Na^+]$ (~0.4–0.6 M) but similar $\Omega_{calcite}$ (11.5 ± 0.5). (a) $(Na/Ca)_c$ vs solution $(Na^+)^2/Ca^{2+}$ activity ratio. (b) $(Na/Ca)_c$ vs $\log R_c$. Uncertainties in $\log R_c$ values (error bars) are mostly due to the uncertainty in the surface area of calcite crystals during the course of an experiment. These results indicate both crystal growth rate and the solution $(Na^+)^2/Ca^{2+}$ activity ratio affected $(Na/Ca)_c$ and small differences in crystal growth rates among experiments resulted in significant differences in $(Na/Ca)_c$.

but near-constant a_{Na^+} and crystal growth rates (Fig. 3, $\log R_c = -5.25$ to -5.11 mol/m²/s). Overall, our inorganic calcite results indicate a 0.22% increase in $(Na/Ca)_c$ per % increase in $a^2_{Na^+}/a_{Ca^{2+}}$ (Fig. 2a; Eq. (13)).

A $a^2_{Na^+}/a_{Ca^{2+}}$ control on $(Na/Ca)_c$ is also consistent with recent results from synchrotron X-ray spectroscopy analyses of biogenic calcite and aragonite minerals showing that Na^+ is bound to CO_3^{2-} in the calcite lattice in the form of Na_2CO_3, implying a substitution of Ca^{2+} by Na^+ (Yoshimura et al., 2017). Although the exact substitution mechanism remains to be elucidated, a $a^2_{Na^+}/a_{Ca^{2+}}$ control on $(Na/Ca)_c$ makes it sensible to express the results on Na^+ partitioning in terms of the distribution coefficient D_{Na}:

$$D_{Na} = \frac{(Na/Ca)_c}{a^2_{Na^+}/a_{Ca^{2+}}}, \quad (14)$$

Here D_{Na} is expressed using free ionic activities following Lippmann (1980). Using ionic concentrations instead of free activities results in a similar level of data-model agreement (not shown). Combining Eq. (13) with Eq. (14), the following power law is obtained for D_{Na} (Fig. 2b):

$$D_{Na} = \Delta\left(a^2_{Na^+}/a_{Ca^{2+}}\right)^{k-1}. \quad (15)$$

The decrease in D_{Na} (2.8×10^{-4}–1.5×10^{-5}) as $a^2_{Na^+}/a_{Ca^{2+}}$ increases from 2.0 to 125 (Fig. 2b) is reminiscent of the partitioning behaviour of Mg^{2+} in calcite, with D_{Mg} decreasing with increasing $a_{Mg^{2+}}/a_{Ca^{2+}}$ (e.g. Mucci and Morse, 1983) but contrasts with the behaviour of Sr^{2+} and Ba^{2+}, which display constant partitioning coefficients with respect to the solution $a_{Sr^{2+}}/a_{Ca^{2+}}$ and $a_{Ba^{2+}}/a_{Ca^{2+}}$, respectively (e.g. Tesoriero and Pankow, 1996). We speculate that the negative covariation between D_{Na} and $a^2_{Na^+}/a_{Ca^{2+}}$ may be caused by a decreasing availability of CO_3^{2-} vacancies as more Na^+ is incorporated.

4.1.2. Crystal growth rate

Calcite and aragonite crystal growth rates affect the incorporation of trace-elements into the crystal lattice (McIntire, 1963). Early work on sodium incorporation into inorganic calcite by Busenberg and Plummer (1985) showed a doubling in $(Na/Ca)_c$ per order of magnitude change in crystal growth rate. However, variable amounts of sulphate-bearing ions in their calcite samples did not allow for assessing the effect of crystal growth rate independently of the effect of sulphates. Recent work by Füger et al. (2019) also demonstrated a strong crystal growth rate effect on calcite D_{Na} but the effect of $a^2_{Na^+}/a_{Ca^{2+}}$ on D_{Na} was not assessed, limiting the quantification of crystal growth rate effects.

The results from this study confirm that Na^+ incorporation into calcite greatly increases with higher R_c values (Fig. 3). Four of the chemostat experiments (35_10, 11, 17, 18) were conducted under a very similar $a^2_{Na^+}/a_{Ca^{2+}}$ of 643 ± 8 but with variable calcite growth rate (Fig. 3, $\log R_c = -6.0$ to -5.2 mol/m²/s, Table 1). From this set of experiments, a fivefold increase in $(Na/Ca)_c$ per order of magnitude increase in R_c is inferred (Fig. 3). This result suggests a much stronger crystal growth rate effect on $(Na/Ca)_c$ than previously reported by Busenberg and Plummer (1985), suggesting that the relation between $(Na/Ca)_c$ and R_c may not be linear. Calcite growth rate effects on the partitioning of a cation substituting for Ca^{2+} have been explained by surface kinetic models (Watson, 2004; DePaolo, 2011). These models successfully reproduce the rate dependence observed for doubly-charged ions (e.g. Sr^{2+}, Mn^{2+}, DePaolo, 2011) but have not been applied to monovalent ions like Na^+ because the mode of incorporation into calcite remained unclear. Results from recent work on inorganic and biogenic $CaCO_3$ (Yoshimura et al., 2017; Hauzer et al., 2018; Zhou et al., 2021) suggest Na^+ substitutes for Ca^{2+} in calcite and aragonite. The DePaolo (2011) model predicts that the incorporation of impurity ions substituting for Ca^{2+} into calcite is controlled by the calcite dissolution/precipitation ratio (R_b/R_f). Following DePaolo (2011), the partitioning of Na^+ between calcite and solution may be described as follows:

$$D_{Na} = \frac{D_{Na}^f}{1 + \frac{R_b}{R_f}\left(\frac{D_{Na}^f}{D_{Na}^{eq}} - 1\right)}, \quad (16)$$

where D_{Na}^f and D_{Na}^{eq} are Na^+ distribution coefficients for the kinetic and equilibrium limits, respectively, and R_b/R_f is the $CaCO_3$ dissolution/precipitation reaction rate ratio.

Our results indicate D_{Na} is not a constant at a given R_c but depends on $a_{Na^+}^2/a_{Ca^{2+}}$ (Fig. 2b, Eq. (15)). To accommodate for the $a_{Na^+}^2/a_{Ca^{2+}}$ dependence of D_{Na}, we express D_{Na}^f and D_{Na}^{eq} as functions of $a_{Na^+}^2/a_{Ca^{2+}}$ by substituting Eq. (15) into (16) and obtain the following relation for D_{Na}:

$$D_{Na} = \frac{\Delta_f \left(a_{Na^+}^2/a_{Ca^{2+}}\right)^{k_f-1}}{1 + \frac{R_b}{R_f}\left(\frac{\Delta_f \left(a_{Na^+}^2/a_{Ca^{2+}}\right)^{k_f-1}}{\Delta_{eq}\left(a_{Na^+}^2/a_{Ca^{2+}}\right)^{k_{eq}-1}} - 1\right)}, \quad (17)$$

where Δ_f, k_f and Δ_{eq}, k_{eq} are best-fit parameters for the dependence of D_{Na} on $a_{Na^+}^2/a_{Ca^{2+}}$ at the kinetic and equilibrium limits respectively. We note that the introduction of an empirical term to the DePaolo (2011) model may limit the predictive power of the model outside the range of conditions described in this study. Results from this study indicate that the relative sensitivity of $(Na/Ca)_c$ to $a_{Na^+}^2/a_{Ca^{2+}}$ is not strongly altered by R_c. At $R_c \sim 10^{-6.3}$ mol/m²/s, $(Na/Ca)_c$ increases by 0.22% per % in $a_{Na^+}^2/a_{Ca^{2+}}$ while at $R_c \sim 10^{-5.2}$, $(Na/Ca)_c$ increases by ~ 0.25% per % in $a_{Na^+}^2/a_{Ca^{2+}}$ (Section 3.2). Hence, it is assumed the k exponents are mostly independent of R_c (i.e. $k_f \sim k_{eq} \sim k = 0.22$) and Eq. (17) simplifies to:

$$D_{Na} = \frac{\Delta_f \left(a_{Na^+}^2/a_{Ca^{2+}}\right)^{k-1}}{1 + \frac{R_b}{R_f}\left(\frac{\Delta_f}{\Delta_{eq}} - 1\right)}. \quad (18)$$

Multiplying Eq. (18) by $a_{Na^+}^2/a_{Ca^{2+}}$, a relation is obtained for $(Na/Ca)_c$:

$$(Na/Ca)_c = \frac{\Delta_f \left(a_{Na^+}^2/a_{Ca^{2+}}\right)^{k}}{1 + \frac{R_b}{R_f}\left(\frac{\Delta_f}{\Delta_{eq}} - 1\right)}. \quad (19)$$

To solve for $(Na/Ca)_c$, the values of Δ_f, Δ_{eq} and R_b/R_f must be known. Here, they are inferred from all the experiments of this study that resulted in the precipitation of 100% calcite ($n = 29$, Table 1). The Δ_{eq} term must be lower than 4.2×10^{-4} (i.e. the value of Δ for the slow-growth experiments, Section 3.1). The R_b/R_f ratio is estimated from the calcite dissolution rate R_b in NaCl solution at pH 8–10 and 25 °C ($10^{-7.2}$ to $10^{-6.2}$ mol/m²/s, Chou et al., 1989; Ruiz-Agudo et al., 2010) and the forward rate is derived from the measured net precipitation rate R_c and the backward rate R_b (i.e. $R_f = R_c + R_b$, DePaolo, 2011). A best fit is obtained with $R_b \sim 10^{-7.2}$, $\Delta_{eq} = 6.3 \times 10^{-5}$ and $\Delta_f = 7.4 \times 10^{-3}$ (average data-model difference = 17%, $r^2 = 0.99$, Table 2). Using an R_b value closer to $10^{-6.2}$ mol/m²/s (as in Chou et al., 1989) results in a similar Δ_f value but a higher Δ_{eq} value and an overall worse fit with the data (average data-model difference = 34%, $r^2 = 0.98$).

To investigate the effect of crystal growth rate on $(Na/Ca)_c$ independent of $a_{Na^+}^2/a_{Ca^{2+}}$, we introduce the term F_{R_c}:

$$F_{R_c} = \frac{(Na/Ca)_c}{(Na/Ca)_{c,eq}}, \quad (20)$$

where $(Na/Ca)_{c,eq}$ is the expected value of $(Na/Ca)_c$ under near chemical equilibrium conditions. Following the formulation of Eq. (13) for $(Na/Ca)_c$, $(Na/Ca)_{c,eq}$ is expressed as follows:

$$(Na/Ca)_{c,eq} = \Delta_{eq}\left(a_{Na^+}^2/a_{Ca^{2+}}\right)^k. \quad (21)$$

Substituting Eqs. (19) and (21) into (20), the following relation is obtained for F_{R_c}:

$$F_{R_c} = \left(\frac{\Delta_{eq}}{\Delta_f} + \frac{R_b}{R_f}\left(1 - \frac{\Delta_{eq}}{\Delta_f}\right)\right)^{-1}. \quad (22)$$

Table 2
Model best-fit values for $(Na/Ca)_c$ prediction.

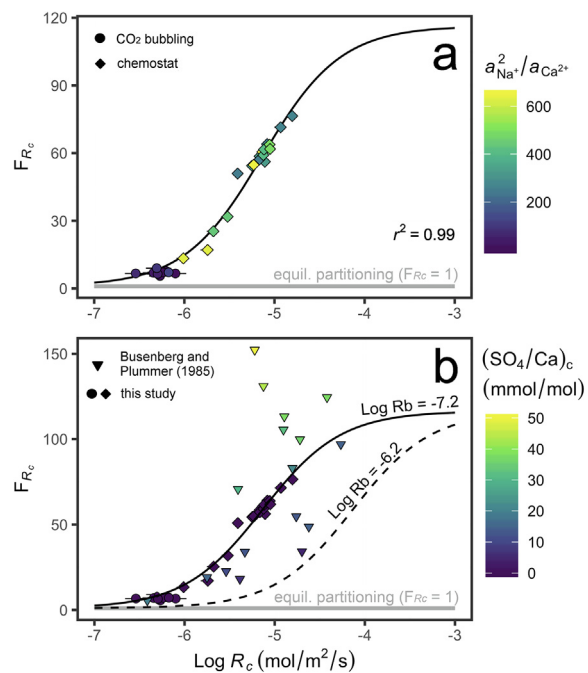| Constant	Value	Unit	r^2	n	p-value
k	0.22	–	0.99	34	$<10^{-4}$
R_b	$10^{-7.2}$	mol/m²/s			
Δ_{eq}	6.3×10^{-5}	–			
Δ_f	7.4×10^{-3}	–			

Fig. 5. Effect of crystal growth rate on calcite Na/Ca expressed with the term F_{R_c} (i.e. the effect of the solution $(Na^+)^2/Ca^{2+}$ activity ratio on $(Na/Ca)_c$ was removed; see Eqs. (20)–(22)). (a) Results for all the calcite experiments carried in this study and best-fit line (continuous black curve) obtained with Eq. (22) and $R_b = 10^{-7.2}$ mol/m²/s, $\Delta_{eq} = 6.3 \times 10^{-5}$ and $\Delta_f = 7.4 \times 10^{-3}$. This panel shows a crystal growth rate effect on calcite Na/Ca that is independent of the solution $(Na^+)^2/Ca^{2+}$ activity ratio. (b) same as (a) but with additional data calculated from the Busenberg and Plummer (1985) calcite experiments. The effect of calcite SO_4/Ca on $(Na/Ca)_c$ is apparent. F_{R_c} values that are significantly lower than the continuous black curve may be explained by lower R_b values (e.g. dotted black curve obtained with $R_b = 10^{-6.2}$ mol/m²/s). Uncertainties in $\log R_c$ values (error bars) are mostly due to the uncertainty in the surface area of calcite crystals during the course of an experiment.

The value of F_{R_c} represents the increase in Na^+ uptake into $CaCO_3$ caused by crystal growth rate relative to Na^+ uptake at near-equilibrium conditions. By definition F_{R_c} equals 1 at chemical equilibrium and increases up to a value equal to $\frac{\Delta_f}{\Delta_{eq}}$ at the kinetic limit of Na partitioning. Computed F_{R_c} values from measured $(Na/Ca)_c$ display a clear relationship with R_c with little scatter and no discernible $a^2_{Na^+}/a_{Ca^{2+}}$ effect (Fig. 5a). Data obtained from the calcite samples show F_{R_c} increases ~14 fold over the -6.5 to -4.7 $mol/m^2/s$ range in $\log R_c$ (Fig. 5a), representing more than an order of magnitude increase in $(Na/Ca)_c$ induced by crystal growth rate effects. The inferred increase in $(Na/Ca)_c$ from calcite samples likely does not cover the full range of the crystal growth rate effect. Modelled F_{R_c} using Eq. (22) agree well with calcite data (Fig. 5a, $r^2 = 0.99$) and could potentially suggest a ~100 fold increase in $(Na/Ca)_c$ from equilibrium ($R_c < 10^{-7}$ $mol/m^2/s$) to the kinetic limit ($R_c > 10^{-3}$ $mol/m^2/s$).

4.1.3. Carbonate sulphate content

Sodium concentration in calcite and aragonite has been shown to increase with the amount of sulphate ions incorporated in the crystal lattice (Kitano et al., 1975; Busenberg and Plummer, 1985) possibly due to the effect of sulphates on lattice parameters (e.g. Goetschl et al., 2019). Previously published $(Na/Ca)_c$ data from inorganic calcite samples with variable SO_4/Ca ratios (Busenberg and Plummer, 1985) are compared to the data presented in this study in Fig. 5b. Overall, $(Na/Ca)_c$ increases with a sample's sulphate content, where $(SO_4/Ca)_c > 20$ mmol/mol. The Busenberg and Plummer (1985) samples with $(SO_4/Ca)_c < 20$ mmol/mol are either in good agreement with the data presented in this study or have lower $(Na/Ca)_c$ ratios than expected from Eq. (22) with $R_b = 10^{-7.2}$ (Fig. 5b). These lower $(Na/Ca)_c$ values (i.e. F_{Rc} in Fig. 5b) could potentially be explained by higher and variable R_b values ($10^{-6.2} < R_b < 10^{-7.2}$).

4.1.4. General model for calcite Na/Ca

For calcite samples with $(SO_4/Ca)_c < 20$ mmol/mol, $(Na/Ca)_c$ has been expressed as a function of the solution $a^2_{Na^+}/a_{Ca^{2+}}$ and R_c:

$$(Na/Ca)_c = F_{R_c} \cdot \Delta_{eq} \left(a^2_{Na^+}/a_{Ca^{2+}} \right)^k. \quad (23)$$

Model outputs using Eq. (23) with the parameter values listed in Table 2 are compared to measured $(Na/Ca)_c$ for all inorganic $CaCO_3$ samples precipitated in this study and the calcite samples with $(SO_4/Ca)_c < 20$ mmol/mol from the study of Busenberg and Plummer (1985) (Fig. 6, $r^2 = 0.91$). The comparison of model outputs with the Busenberg and Plummer (1985) data provides an independent way of testing the predictive power of the model since these data were not used to derive model parameters. The model satisfactorily predicts the $(Na/Ca)_c$ data from the study of Busenberg and Plummer (1985), therefore encouraging model applications to other studies and calcite material. Overall, these results suggest the $(Na/Ca)_c$ of low

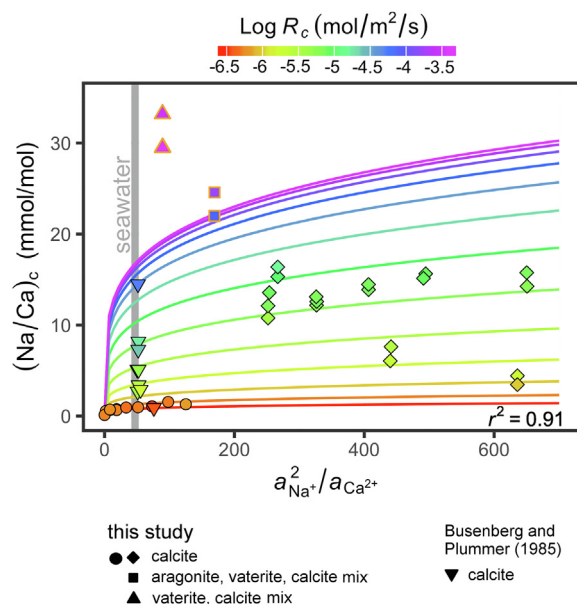Fig. 6. Combined effect of the solution $(Na^+)^2/Ca^{2+}$ activity ratio and crystal growth rate ($\log R_c$) on the sodium content of calcium carbonate minerals $(Na/Ca)_c$. Measured $(Na/Ca)_c$ (coloured data points: this study and the Busenberg and Plummer (1985) experiments with $(SO_4/Ca)_c < 20$ mmol/mol) are compared to model outputs (coloured lines). Model outputs were obtained with Eq. (23) and $R_b = 10^{-7.2}$ $mol/m^2/s$, $\Delta_{eq} = 6.3 \times 10^{-5}$ and $\Delta_f = 7.4 \times 10^{-3}$ (i.e. same parameter values as in Fig. 5a). Data related to experiments with aragonite and/or vaterite co-precipitation (orange outline) and calcite data from the Busenberg and Plummer (1985) study were not used to derive model parameters but are shown for comparison.

Mg-calcite with $(SO_4/Ca)_c < 20$ mmol/mol could potentially be used as a proxy for crystal growth rate and the solution $a^2_{Na^+}/a_{Ca^{2+}}$.

4.1.5. Calcium carbonate polymorphs

Results from previously published inorganic $CaCO_3$ experiments suggest higher Na^+ uptake in aragonite than in calcite (Kitano et al., 1975) but similar Na^+ partitioning for low and high Mg-calcite (White, 1978). A few samples analysed in this study contained significant proportions of aragonite (~40%) and vaterite (up to 14–35%). These latter samples were all obtained from solutions having higher saturation levels with respect to calcite ($45 < \Omega_{calcite} < 190$, Table 1) and display significantly higher $(Na/Ca)_c$ values than the pure calcite samples despite the former precipitating from solutions with comparatively low $a^2_{Na^+}/a_{Ca^{2+}}$ (Fig. 3).

Experiments carried out with a solution $\Omega_{calcite}$ of 180–190 resulted in mixtures of calcite and vaterite (CV samples, Table 1). It is expected that amorphous calcium carbonate (ACC) precursors formed during these experiments since the ACC solubility product was attained during these experiments ($K_{sp\_ACC} \sim 4 \times 10^{-7} \sim 120$ $K_{sp\_calcite}$ at 25 °C, Brecevic and Nielsen, 1989). The $(Na/Ca)_c$ values of the CV samples (~29–33 mmol/mol) are the highest of all samples analysed in this study and cannot be explained

by the DePaolo (2011) kinetic model using the parameters derived with the calcite samples (Fig. 6). These high (Na/Ca)$_c$ values are interpreted to reflect enhanced Na$^+$ uptake in vaterite and/or ACC compared to calcite.

Samples containing a mixture of calcite, aragonite and vaterite (CAV samples, Table 1) formed in solutions with $\Omega_{calcite}$ of 45–50. Although the (Na/Ca)$_c$ results of the CAV samples are in good agreement with modelled (Na/Ca)$_c$ using the model parameters as derived from experiments with pure calcite samples (Fig. 6), the presence of three CaCO$_3$ polymorphs limits the interpretation of the (Na/Ca)$_c$ results for these samples.

4.1.6. Alternative model for calcite Na/Ca

A significantly distinct model of Na$^+$ partitioning between calcite and solution involving a bicarbonate ion control on D_{Na} has been postulated based on a reported correlation between D_{Na} and the activity of HCO$_3^-$ ions (Füger et al., 2019). According to this model, HCO$_3^-$ compensates for the charge imbalance resulting from the assim-

ilation of Na$^+$ into calcite, presumably by assimilation of the NaHCO$_3^0$ ion pair present in solution (Füger et al., 2019). Results from this study indicate variations in D_{Na} at a given R_c value are poorly explained by either the activity of HCO$_3^-$ ions (Fig. 7a–c) or the HCO$_3^-$/Na$^+$ activity ratio (Fig. 7d–f). In fact, at a given R_c value, experiments with the highest HCO$_3^-$ activities have the lowest D_{Na} values (Fig. 7b and c), contradicting the Füger et al. (2019) model. Similarly, a high HCO$_3^-$/Na$^+$ activity ratio does not explain the scatter in D_{Na} values at $R_c \sim 10^{-5.1}$ mol/m^2/s (Fig. 7f).

As shown previously, variations in D_{Na} at a given R_c value are well explained by variations in $a_{Na^+}^2/a_{Ca^{2+}}$ (Section 4.1.1). A low $a_{Na^+}^2/a_{Ca^{2+}}$ promotes high D_{Na} and a high $a_{Na^+}^2/a_{Ca^{2+}}$ promotes low D_{Na} (Fig. 8g–i). Careful examination of the Füger et al. (2019) data suggests solution Na$^+$/Ca^{2+} ratios and HCO$_3^-$ activities covaried negatively, potentially explaining the positive relationship between calcite D_{Na} and HCO$_3^-$ activity reported by these authors.
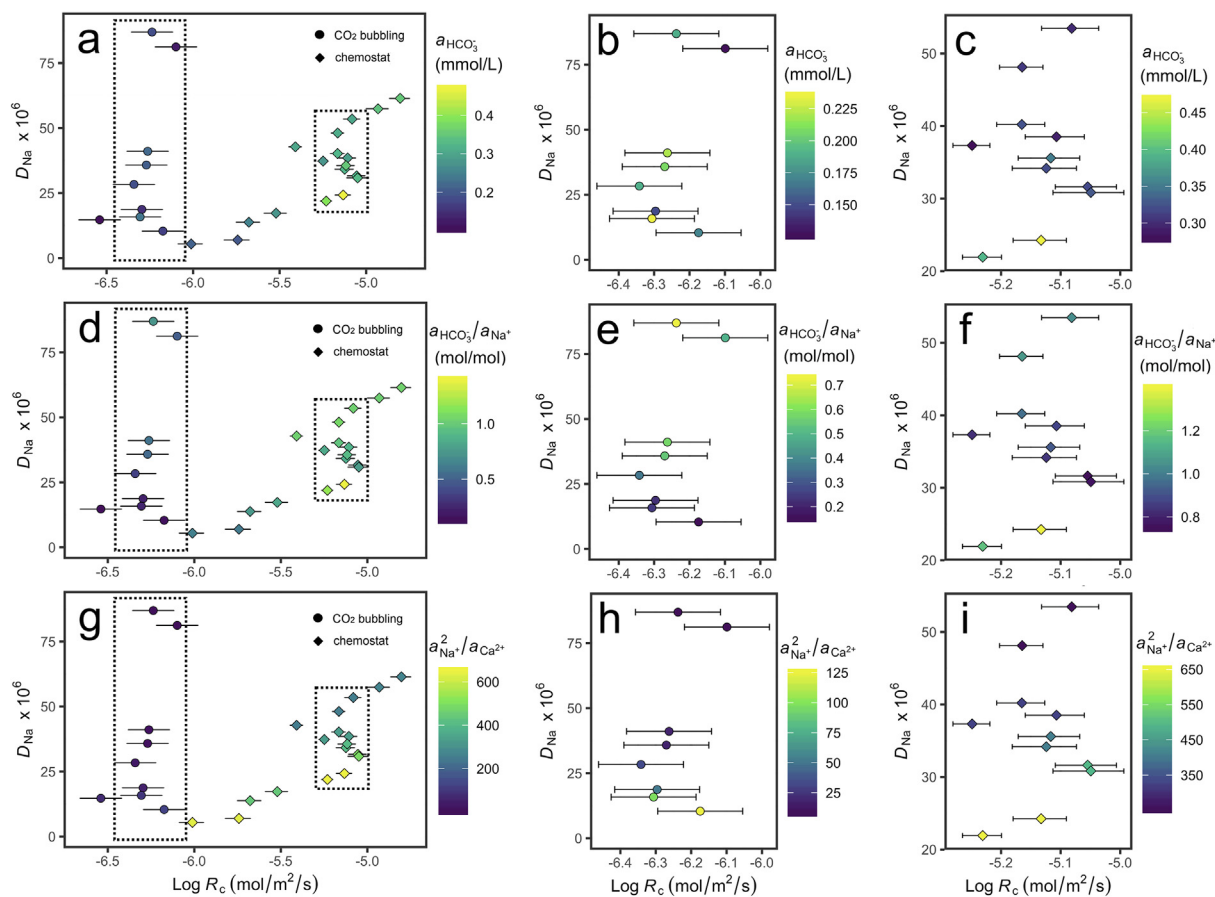

Fig. 7. Effect of crystal growth rate (LogR_c) and the solution HCO$_3^-$ activity (a, b, c), HCO$_3^-$/Na$^+$ activity ratio (d, e, f) and (Na$^+$)^2/Ca^{2+} activity ratio (g, h, i) on the partitioning of Na$^+$ between calcite and solution (D_{Na}). Panels on the left side (a, d, g) show all the calcite D_{Na} values calculated from this study's experiments (except S7 and S8 with $D_{Na} > 2 \times 10^{-4}$ due to very low solution (Na$^+$)^2/Ca^{2+} activity ratios). Panels in the middle (b, e, h) provide more details for experiments with Log$R_c = -6.4$ to -6.0 mol/m^2/s. Panels on the right side (c, f, i) provide more details for experiments with Log$R_c = -5.3$ to -5.0 mol/m^2/s. The error bars for logR_c values represent the uncertainty in the surface area of calcite crystals during the course of an experiment. This figure shows D_{Na} is not significantly affected by the activity of HCO$_3^-$ ions or the HCO$_3^-$/Na$^+$ activity ratio (a proxy for the NaHCO$_3^0$/Na$^+$ ratio). The scatter in D_{Na} at a given LogR_c is explained by variations in the solution (Na$^+$)^2/Ca^{2+} activity ratio.
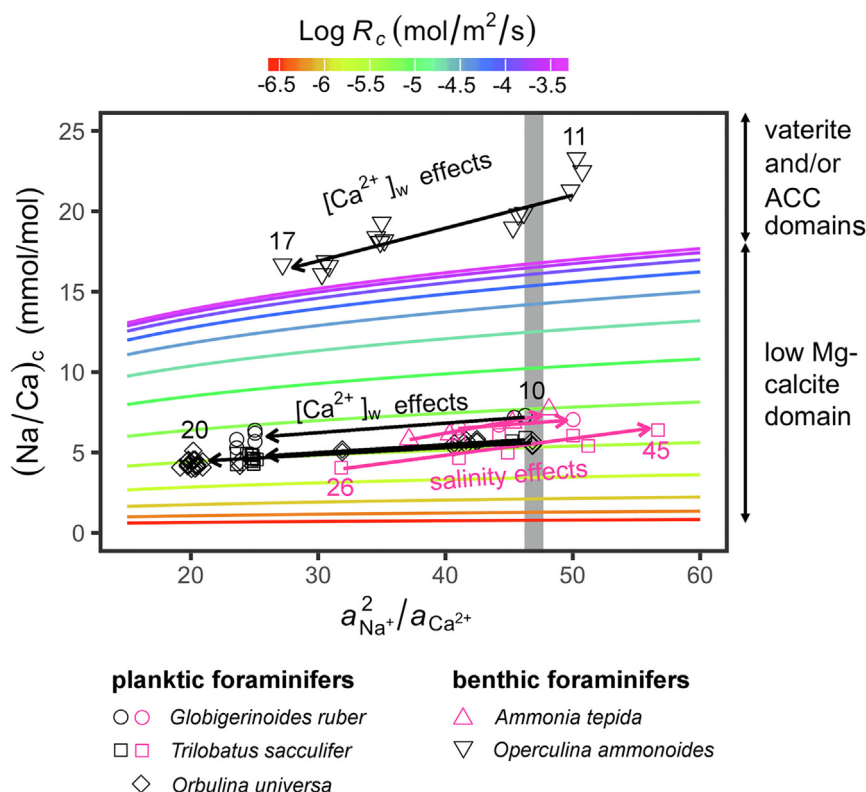
Fig. 8. Published foraminifer Na/Ca ratios from culture experiments explained in terms of variable seawater $(Na^+)^2/Ca^{2+}$ activity ratios $(a_{Na^+}^2/a_{Ca^{2+}})$ and calcite growth rate ($LogR_c$). The standard seawater $a_{Na^+}^2/a_{Ca^{2+}}$ (47; DOE, 1994) is indicated by the grey vertical line. Where seawater $[Ca^{2+}]$ is altered ($[Ca^{2+}] = 10$ to 20 mM, black data symbols), the sensitivities of planktic $(Na/Ca)_{foraminifer}$ (Zhou et al., 2021) to $a_{Na^+}^2/a_{Ca^{2+}}$ (+0.23 to + 0.26% per % in $a_{Na^+}^2/a_{Ca^{2+}}$) are very similar to that of low-Mg inorganic calcite precipitated at $LogR_c = -5.5$ to -5.3 to mol/m^2/s (+0.22% per % in $a_{Na^+}^2/a_{Ca^{2+}}$). Where salinity is altered (26 to 45 g/kg; pink data symbols: *A. Tepida*, Wit et al., 2013; *G. Ruber*, Allen et al., 2016; *T. sacculifer*, Allen et al., 2016; Bertlich et al., 2018), a positive covariation between salinity and foraminiferal calcite growth rates can explain why planktic and benthic $(Na/Ca)_{foraminifer}$ have an apparent higher sensitivity to $a_{Na^+}^2/a_{Ca^{2+}}$ than low-Mg inorganic calcite precipitated at constant R_c. The precipitation of vaterite and/or amorphous calcium carbonate prior to calcite transformation may explain the comparatively high $(Na/Ca)_{O.\ ammonoides}$ ratios (Hauzer et al., 2018).

4.2. Implication for natural carbonates

4.2.1. Biogenic $(Na/Ca)_c$ as an indicator of seawater calcium concentration

Fossil foraminifer and coral $(Na/Ca)_c$ values have been suggested to reflect past changes in seawater calcium concentrations because the $(Na/Ca)_c$ of these taxa is positively correlated with the environmental Na^+/Ca^{2+} concentration ratio (Gothmann et al., 2015; Hauzer et al., 2018; Zhou et al., 2021) and the residence time of Ca^{2+} in the ocean is short (~1 My) relative to that of Na^+ (~100 My). In particular, foraminiferal $(Na/Ca)_c$ decreased with increasing $[Ca^{2+}]_w$ in studies where benthic (Hauzer et al., 2018) and planktic (Zhou et al., 2021) species were cultured in natural seawater with and without the addition of $CaCl_2$. The present study shows that the $(Na/Ca)_c$ of inorganic calcite is positively correlated with the solution $a_{Na^+}^2/a_{Ca^{2+}}$ and the crystal growth rate (Fig. 6) as well as the calcite sulphate content (Fig. 5b). Sulphate concentrations in low-Mg foraminiferal calcite are commonly below 20 mmol/mol (e.g. Busenberg and Plummer, 1985), a level which does not seem to increase $(Na/Ca)_c$ significantly (Fig. 5b). An

increase in $[Ca^{2+}]_w$ is expected to decrease the $a_{Na^+}^2/a_{Ca^{2+}}$ but increase the $\Omega_{calcite}$ of the calcifying fluid (CF). For example, a ~ 70% decrease in seawater $a_{Na^+}^2/a_{Ca^{2+}}$ caused by the addition of $CaCl_2$ salt (as in the Hauzer et al., 2018 experiment) could be expected to result in a ~70% increase in $\Omega_{calcite}$ assuming $[Ca^{2+}]$ in the CF is proportional to the environmental $[Ca^{2+}]_w$. In turn, an increase in $\Omega_{calcite}$ would lead to an increase in crystal growth rate and Na^+ uptake in the calcite lattice. Hence, it could be expected that a higher seawater $[Ca^{2+}]_w$ leads to competing and opposite effects on $(Na/Ca)_c$, with a lower environmental $a_{Na^+}^2/a_{Ca^{2+}}$ causing a lower $(Na/Ca)_c$ but a higher crystal growth rate causing a higher $(Na/Ca)_c$. However, the sensitivity of low-Mg planktic foraminifer $(Na/Ca)_c$ to seawater $a_{Na^+}^2/a_{Ca^{2+}}$ (+0.23 to +0.26% per % in $a_{Na^+}^2/a_{Ca^{2+}}$, Fig. 8) is similar that of inorganic calcite $(Na/Ca)_c$ (+0.22%, Fig. 8), suggesting that environmental $[Ca^{2+}]_w$ does not affect biomineral growth rates significantly for these taxa.

The $(Na/Ca)_c$ ratio of benthic foraminifer *Operculina ammonoides* ($(Na/Ca)_{O.\ ammonoides}$: 16 to 21 mmol/mol, Hauzer et al., 2018) is also positively correlated with seawa-

ter $a_{Na^+}^2/a_{Ca^{2+}}$ but sits significantly higher than the range of $(Na/Ca)_c$ covered by low Mg-calcite planktic species as well as the range expected for low-Mg inorganic calcite (Fig. 8). The significantly higher $(Na/Ca)_{O.\ ammonoides}$ ratios suggest Na^+ partitioning for this species may reflect the formation of (a) precursor phase(s) (i.e. ACC and/or vaterite) and/or a possible enhanced Na^+ uptake in calcite with high Mg or SO_4. Nevertheless, $a_{Na^+}^2/a_{Ca^{2+}}$ appears to be the primary variable controlling $(Na/Ca)_{O.\ ammonoides}$, with no evidence for a significant crystal growth rate effect caused by higher seawater $[Ca^{2+}]_w$. Regardless of the potential causes for the absence of a positive $[Ca^{2+}]_w$ effect on foraminifer $(Na/Ca)_c$, the similar $a_{Na^+}^2/a_{Ca^{2+}}$ sensitivities for foraminifer and inorganic calcite $(Na/Ca)_c$ are encouraging and should promote further development of this proxy. Further testing the sensitivity of foraminifer $(Na/Ca)_c$ to seawater $[CO_3^{2-}]_w$, $[DIC]_w$ and $[Mg^{2+}]_w$ is necessary since these variables have changed significantly in the geologic past (e.g. Zeebe, 2012) and could potentially impact biomineralization rates and Na^+ uptake in calcite.

4.2.2. Biogenic $(Na/Ca)_c$ as an indicator of seawater salinity

The sodium content of the calcium carbonate shells or skeletons of marine calcifiers has been shown to increase with the salinity of the environment in which biomineralization occurs (Ishikawa and Ichikuni, 1984). In particular, foraminiferal calcite $(Na/Ca)_c$ is significantly correlated with seawater salinity (Wit et al., 2013; Mezger et al., 2016, 2018, 2019; Allen et al., 2016; Bertlich et al., 2018; Geerken et al., 2018) but the cause(s) of this covariation has not been determined. Planktic foraminifers cultured in seawater of various salinity (26 to 45 g/kg) display $(Na/Ca)_c$ ratios with enhanced sensitivity to $a_{Na^+}^2/a_{Ca^{2+}}$ (e.g. *T. sacculifer*: +0.48% per % in $a_{Na^+}^2/a_{Ca^{2+}}$, Fig. 8) compared to the $(Na/Ca)_c$ of inorganic calcite precipitated under constant R_c (+0.22%) and the $(Na/Ca)_c$ of the same taxa cultured in seawater with altered $[Ca^{2+}]_w$ (*T. sacculifer*: +0.26%). This suggests more than half of the salinity effect on *T. sacculifer* $(Na/Ca)_c$ is caused by a variable other than $a_{Na^+}^2/a_{Ca^{2+}}$. An increase in seawater salinity from 26 to 45 g/kg (as in Bertlich et al., 2018) with a constant Na^+/Ca^{2+} concentration ratio results in $a_{Na^+}^2/a_{Ca^{2+}}$ increasing almost proportionally from 34 to 61 (Fig. 9a). Model results suggest this would lead to a +14% increase in $(Na/Ca)_c$, which is significantly lower than the +47% to +100% increase in $(Na/Ca)_c$ reported for *T. sacculifer* (Mezger et al., 2016; Bertlich et al., 2018). We postulate that higher salinities lead to higher $\Omega_{calcite}$ in the calcifying fluid of foraminifers, which in turns leads to higher crystal growth rates and Na^+ uptake by calcite. Over the 26–45 g/kg salinity range, $\Omega_{calcite}$ of a foraminifer CF could potentially double (Fig. 9b) assuming a CF composition similar to environmental seawater but with an elevated pH (i.e. pH = 8.6–9.0, Bentov et al., 2009; de Nooijer et al., 2009a, 2009b; Toyofuku et al., 2017). A doubling of $\Omega_{calcite}$ in seawater at 25 °C results in a ~ fourfold increase in crystal growth rate (Lopez et al., 2009; Wolthers et al., 2012), which in turns leads to an approximate doubling in $(Na/Ca)_c$ for $LogR_c$ values above −5.7 mol/m²/s (Figs. 5a and 8). Thus,
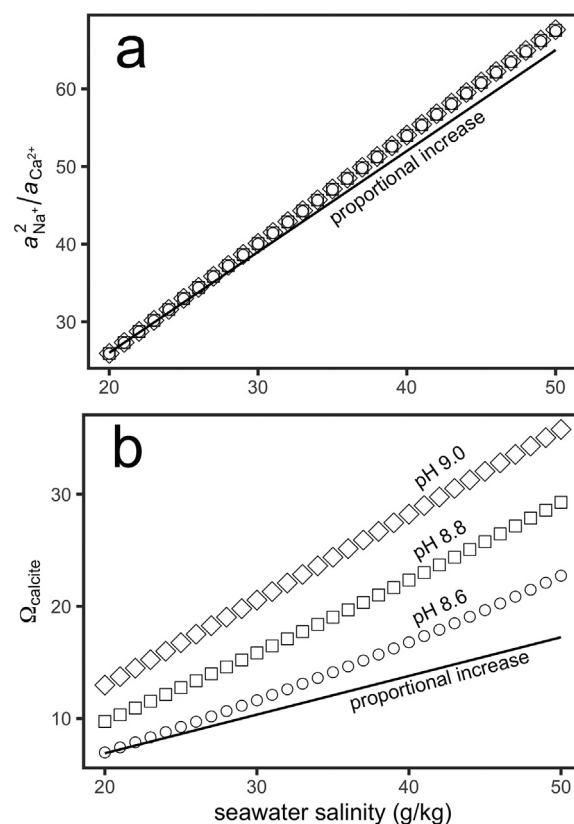
Fig. 9. Simulated chemical conditions in the calcifying fluid of a foraminifer as a function of salinity assuming a calcifying fluid pH of 8.6–9.0 (de Nooijer et al., 2009a, 2009b) and $[Na^+]$ and $[Ca^{2+}]$ identical to the environmental seawater. (a) Effect of salinity on the $(Na^+)^2/Ca^{2+}$ activity ratio ($a_{Na^+}^2/a_{Ca^{2+}}$). (b) Effect of salinity on $\Omega_{calcite}$. This figure suggests that variations in $(Na/Ca)_{foraminifer}$ caused by variations in salinity originate from positive covariations between salinity and a foraminifer calcifying fluid's $a_{Na^+}^2/a_{Ca^{2+}}$ and $\Omega_{calcite}$. Small variations in a foraminifer calcifying fluid's pH likely impact $\Omega_{calcite}$ and $(Na/Ca)_{foraminifer}$.

the expected impact of $\Omega_{calcite}$ on $(Na/Ca)_c$ caused by increasing salinity is potentially stronger than the effect caused by seawater $a_{Na^+}^2/a_{Ca^{2+}}$ discussed earlier. We therefore postulate that reported increases in foraminiferal $(Na/Ca)_c$ with increasing seawater salinities are caused in large part by a covariation between salinity and the biomineral growth rate. Taxonomic and between-studies differences in foraminiferal '$(Na/Ca)_c$ vs salinity' relationships may therefore indicate a variable response of internal carbonate chemistry and/or pH (and therefore $\Omega_{calcite}$) to changes in salinity. Modelled results suggest the reported increase in $(Na/Ca)_{T.\ sacculifer}$ with salinity (~4.1 to 6.4 mmol/mol, Bertlich et al., 2018) could correspond to a salinity-induced increase in crystal growth rate from ~$10^{-5.6}$ to $10^{-5.4}$ mol/m²/s (Fig. 8). Extrapolating this reasoning to other element-to-calcium ratios suggests foraminiferal Sr/Ca, Ba/Ca, B/Ca and Li/Ca should also be positively correlated with salinity since the incorporations of these trace elements in calcite are positively affected by crystal growth rates (e.g. Gabitov et al., 2019). Evidence for positive correlations between foraminiferal calcite

Sr/Ca and salinity (Kisakurek et al., 2008; Duenas-Bohorquez et al., 2009; Dissard et al., 2010; Wit et al., 2013) supports the 'crystal growth rate' hypothesis.

These assessments depend somewhat on whether Na^+ and Ca^{2+} concentrations in the foraminifer CF are similar to seawater, which may not be the case due to the role of selective ion transport (Bentov and Erez, 2006; Nehrke et al., 2013; de Nooijer et al., 2014) and the uptake of Ca^{2+} during calcification. However, active Ca^{2+} transport and calcification are unlikely to alter the concentrations of Na^+ and Ca^{2+} in the CF by more than a few percent (e.g. Furla et al., 2000) because Na^+ is highly concentrated in seawater (~0.47 M) and Ca^{2+} is not expected to be the limiting factor for biomineralization (as opposed to CO_3^{2-} ions which are significantly less concentrated than Ca^{2+} in seawater).

4.2.3. Crystal growth rates of biogenic calcium carbonate minerals

The strong positive covariation between inorganic calcite Na/Ca and crystal growth rate (Fig. 3) and the moderate $(Na/Ca)_c$ sensitivity to changes in $a^2_{Na^+}/a_{Ca^{2+}}$ (Figs. 6 and 8) suggest calcite Na/Ca may provide some constraints on crystal growth rates for natural calcite with SO_4/Ca lower than ~20 mmol/mol (cf. Fig. 5b). Maximum crystal growth rates for a selection of marine calcifiers were estimated based on published $(Na/Ca)_c$ data (Fig. 10, Table 3) and assuming the calcifying fluid $a^2_{Na^+}/a_{Ca^{2+}}$ reflects the modern seawater value of 47 (DOE, 1994). It is also assumed that the involvement of Mg^{2+} at the site of calcification does not alter the effect of growth rate on Na^+ incorporation considerably. Overall, inferred crystal growth rates for marine calcifiers vary from $10^{-5.6}$ to above $10^{-4.0}$ mol/m^2/s. This range in crystal growth rate is consistent with the idea that kinetic rather than equilibrium processes determine trace-element partitioning and isotopic fractionation between biominerals and seawater (Watson, 2004; DePaolo, 2011; Watkins et al., 2013, 2014; Devriendt et al., 2017a, 2017b).

Among marine calcifiers, sea pens, sea urchins, sand dollar and green spine are expected to exhibit some of the highest growth rates ($\log R_c > -4.0$ mol/m^2/s), followed by calcitic corals (gorgonians), bivalves, red algae, high-Mg benthic foraminifers, coraline algae and oysters ($\log R_c > -5.0$ mol/m^2/s) while slowest crystal growth rate are inferred for coccoliths and low-Mg foraminifers ($-5.6 < \log R_c < -5.2$ mol/m^2/s). The inferred precipitation rates for sea urchins, which are beyond the limit of Na^+ kinetic partitioning for calcite, are consistent with observations that show ACC as a precursor (Beniash et al., 1997; Politi et al., 2004). The Na/Ca of foraminifers generally suggest lower crystal growth rates, although the benthic species *Operculina ammonoides* has $(Na/Ca)_c$ values that could suggest relatively high precipitation rates ($\log R_c > -4.0$ mol/m^2/s). This particular species has a shell made of high Mg-calcite suggesting a different biomineralization pathway (e.g. precipitation of vaterite or ACC in a highly saturated environment) than low-Mg-calcite taxa. Overall, the large $(Na/Ca)_c$ range observed in benthic foraminifera may be explained by the different biomineralization path-
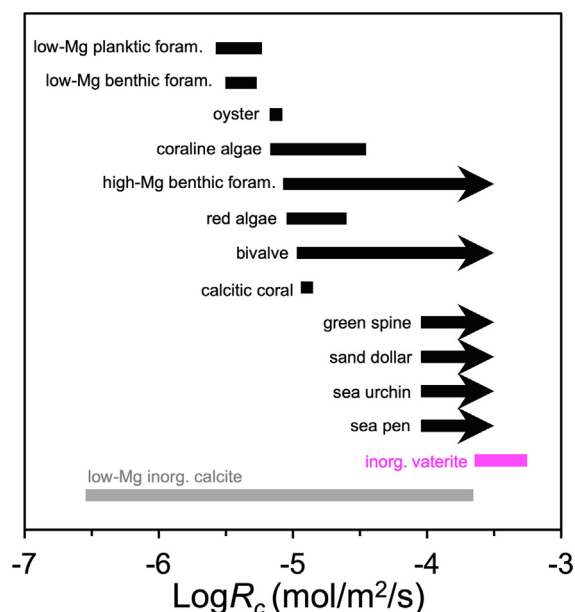

Fig. 10. Maximum calcite growth rate for a range of marine calcifiers inferred from published bulk calcite Na/Ca ratios using Eq. (19) and assuming a constant calcifying fluid $(Na^+)^2/Ca^{2+}$ activity ratio of 47 (i.e. standard seawater, DOE, 1994). Rates were calculated using $R_b = 10^{-7.2}$ mol/m^2/s, $\Delta_{eq} = 6.3 \times 10^{-5}$ and $\Delta_f = 7.4 \times 10^{-3}$ (i.e. same parameter values as in Fig. 5a, Fig. 6 and Fig. 8) and with calcite Na/Ca data from Lorens and Bender, 1980; Busenberg and Plummer (1985); Wit et al. (2013); Mezger et al. (2016); de Moura Neves et al., 2018; Geerken et al. (2018); Hauzer et al. (2018); Zhou et al. (2021) and this study.

ways used by these organisms in contrast to the rather narrow $(Na/Ca)_c$ range in planktic foraminifera.

Within-shell variability in foraminiferal $(Na/Ca)_c$ are characterised by alternating bands of high and low Na/Ca ratios varying by up to 3 fold (Branson et al., 2016; Geerken et al., 2018, 2019; Bonnin et al., 2019). Variations in calcite crystal growth rate of ~ one order of magnitude (e.g. $10^{-6} < R_c < 10^{-5}$ mol/m^2/s) could potentially explain the Na/Ca banding pattern. In addition, the formation of precursor phases such as vaterite during biomineralization (Jacob et al., 2017) could also affect foraminiferal $(Na/Ca)_c$ since vaterite has a significantly higher Na/Ca than calcite when formed under similar $a^2_{Na^+}/a_{Ca^{2+}}$ (Fig. 6). For example, high Na/Ca ratios above 20 mmol/mol reported in parts of foraminiferal shells such as the spines and spine base of spinose foraminifers (Mezger et al., 2018, 2019; Bonnin et al., 2019) could be explained by the formation of vaterite and/or ACC. Taxonomic and temporal variations in the calcifying fluid $a^2_{Na^+}/a_{Ca^{2+}}$ may also contribute to within- and between-shell Na/Ca variability but these effects are less likely to be causing the large differences in Na/Ca between species and within a single shell due to the relatively moderate response of calcite Na/Ca to changes in environmental $a^2_{Na^+}/a_{Ca^{2+}}$ (Fig. 8).

Besides the concentrations of Na^+, Ca^{2+} and SO_4^{2-} in the CF and crystal growth rate effects, additional factors such as the Mg^{2+} concentration, the Mg/Ca ratio and/or

Table 3
Estimated maximum calcite growth rate for a range of marine calcifiers based on published calcite Na/Ca ratios.

Reference	Type	Genus/species	Calcite type	(Mg/Ca)$_c$ mmol/mol	(Na/Ca)$_c$ mmol/mol	logR_c mol/m^2/s
Busenberg and Plummer, 1985	Coral	Gorgonia sp.	High-Mg	123.0	10.9	−4.90
Busenberg and Plummer, 1985	Coralline algae	Gonolithon sp./Lythophyllum	High-Mg	200.0	8.7	−5.12
Busenberg and Plummer, 1985	Coralline algae	?	High-Mg	170.0	13.9	−4.50
Busenberg and Plummer, 1985	Green spines	Echinoderm	High-Mg	77.0	21.7	>−4.00
Busenberg and Plummer, 1985	Red algae	Amphiroa fragilissima	High-Mg	200.0	12.9	−4.65
Busenberg and Plummer, 1985	Red algae	Amphiroa rigida	High-Mg	180.0	9.9	−5.00
Busenberg and Plummer, 1985	Sand dollar	Dentraster	High-Mg	113.0	18.3	>−4.00
Busenberg and Plummer, 1985	Sea urchin (shell)	Diadema	High-Mg	117.0	22.6	>−4.00
Busenberg and Plummer, 1985	Sea urchin (shell)	Lytechinus sp.	High-Mg	117.0	22.2	>−4.00
Busenberg and Plummer, 1985	Sea urchin (shell)	Trypneustes sp.	High-Mg	115.0	21.3	>−4.00
Busenberg and Plummer, 1985	Sea urchin (spine)	Diadema	High-Mg	73.0	22.1	>−4.00
Busenberg and Plummer, 1985	Sea urchin (spine)	Lytechinus sp.	High-Mg	70.0	21.3	>−4.00
Busenberg and Plummer, 1985	Sea urchin (spine)	Trypneustes sp.	High-Mg	84.0	22.2	>−4.00
de Moura Neves et al., 2018	Sea pen	Umbellula	High-Mg	–	36.8	>−4.00
Busenberg and Plummer, 1985	Oyster	Crassostrea virginica	Low-Mg	8.5	8.7	−5.12
Busenberg and Plummer, 1985	Bivalve	Lyropecten nodosus	Low-Mg	2.0	21.9	>−4.00
Lorens and Bender, 1980	Bivalve	Mytilus edulis	Low-Mg	–	10.6	−4.93
Geerken et al., 2018	Benthic foraminifer	Amphistegina lobifera	High-Mg	–	9.6	−5.03
Hauzer et al., 2018	Benthic foraminifer	Operculina ammonoides	High-Mg	–	22.4	>−4.00
Geerken et al., 2018	Benthic foraminifer	Ammonia tepida	Low-Mg	–	5.6	−5.46
Wit et al., 2013	Benthic foraminifer	Ammonia tepida	Low-Mg	–	6.9	−5.31
Allen et al., 2016	Planktic foraminifer	Globigerinoides ruber	Low-Mg	–	6.7	−5.33
Zhou et al., 2021	Planktic foraminifer	Globigerinoides ruber	Low-Mg	–	7.2	−5.28
Allen et al., 2016	Planktic foraminifer	Trilobatus sacculifer	Low-Mg	–	6.1	−5.40
Bertlich et al., 2018	Planktic foraminifer	Trilobatus sacculifer	Low-Mg	–	5.0	−5.53
Zhou et al., 2021	Planktic foraminifer	Trilobatus sacculifer	Low-Mg	–	5.8	−5.43
Zhou et al., 2021	Planktic foraminifer	Orbulina universa	Low-Mg	–	5.5	−5.46

the activity of organic matrices (Branson et al., 2016; Bonnin et al., 2019) in the CF may also influence the Na/Ca of foraminiferal calcite. The large variability in marine biogenic calcite Na/Ca ratios implies that using $(Na/Ca)_c$ ratios for reconstructing either past seawater salinity or Ca^{2+} concentration requires an in-depth knowledge of the biomineralization mechanism for the targeted organism.

5. CONCLUSIONS

Inorganic calcium carbonate crystals were precipitated under different solution $[Na^+]$, $[Ca^{2+}]$ and $[CO_3^{2-}]$ and analysed for their Na/Ca ratios. These experimental results were used to adapt the DePaolo (2011) model to predict calcite Na/Ca as a function of the solution $(Na^+)^2/Ca^{2+}$ activity ratio (White, 1977) and crystal growth rate. Experimental and modelling results lead to the following conclusions:

(1) The partitioning of Na^+ between inorganic calcite and solution at a given crystal growth rate and temperature is not a constant but decreases with the solution $(Na^+)^2/Ca^{2+}$ activity ratio. Calcite Na/Ca increases by 0.22% per % increase in solution $(Na^+)^2/Ca^{2+}$ activity ratio, which is comparable to the sensitivity reported for low-Mg calcite planktic foraminifers but lower than the sensitivity of the high-Mg calcite benthic foraminifer *Operculina ammonoides*.

(2) Calcite Na/Ca increases by at least a factor of ~10 due to crystal growth rate effects for $\log R_c$ values between -6.5 and -4.8 mol/m^2/s.

(3) Calcite Na/Ca increases by a factor of up to 4 due to the presence of sulphate ions in the calcite lattice. However, the Na/Ca of calcite seems unaffected by sulphate ions where the SO_4/Ca ratio is below ~20 mmol/mol.

(4) The use of foraminifer Na/Ca for reconstructing past seawater Ca^{2+} concentration requires testing the independence of foraminifer Na/Ca to the environmental CO_3^{2-} and/or DIC concentrations due to potential positive covariations between these variables and crystal growth rate.

(5) Positive correlations between biogenic calcite Na/Ca and salinity are explained by the positive effect of salinity on both the solution $(Na^+)^2/Ca^{2+}$ activity ratio and crystal growth rate.

(6) Reported biogenic Na/Ca and SO_4/Ca ratios for a range of marine taxa suggest maximum biomineralization rates ranging from $10^{-5.6}$ mol/m^2/s (e.g. planktic foraminifers) to above $10^{-4.0}$ mol/m^2/s (e.g. sea urchins). These inferred crystal growth rates suggest kinetic rather than equilibrium elemental partitioning for most biological calcifiers.

(7) Biogenic calcite with low SO_4/Ca but a Na/Ca ratio above ~20 mmol/mol could indicate vaterite and/or amorphous calcium carbonate preceded the formation of calcite.

Declaration of Competing Interest

The authors declare that they have no known competing financial interests or personal relationships that could have appeared to influence the work reported in this paper.

APPENDIX A. SUPPLEMENTARY MATERIAL

Supplementary data to this article can be found online at https://doi.org/10.1016/j.gca.2021.07.024.

REFERENCES

Allen K. A., Hönisch B., Eggins S. M., Haynes L. L., Rosenthal Y. and Yu J. (2016) Trace element proxies for surface ocean conditions: A synthesis of culture calibrations with planktic foraminifera. *Geochim. Cosmochim. Acta* **193**, 197–221.

Beniash E., Aizenberg J., Addadi L. and Weiner S. (1997) Amorphous calcium carbonate transforms into calcite during sea urchin larval spicule growth. *Proc. R. Soc. Lond. B: Bio. Sci.* **264**, 461–465.

Bentov S. and Erez J. (2006) Impact of biomineralization processes on the Mg content of foraminiferal shells: A biological perspective. *Geochem. Geophys.* **7**.

Bentov S., Brownlee C. and Erez J. (2009) The role of seawater endocytosis in the biomineralization process in calcareous foraminifera. *Proc. Natl. Acad. Sci.* **106**, 21500–21504.

Bertlich J., Nürnberg D., Hathorne E. C., de Nooijer L. J., Mezger E. M., Kienast M., Nordhausen S., Reichart G.-J., Schönfeld J. and Bijma J. (2018) Salinity control on Na incorporation into calcite tests of the planktonic foraminifera Trilobatus sacculifer–Evidence from culture experiments and surface sediments. *Biogeosciences*, 1–38.

Bonnin E. A., Zhu Z., Fehrenbacher J. S., Russell A. D., Hönisch B., Spero H. J. and Gagnon A. C. (2019) Submicron sodium banding in cultured planktic foraminifera Shells. *Geochim. Cosmochim. Acta* **253**, 127–141.

Branson O., Bonnin E. A., Perea D. E., Spero H. J., Zhu Z., Winters M., Hönisch B., Russell A. D., Fehrenbacher J. S. and Gagnon A. C. (2016) Nanometer-scale chemistry of a calcite biomineralization template: implications for skeletal composition and nucleation. *Proc. Natl. Acad. Sci.* **113**, 12934–12939.

Brecevic L. and Nielsen A. E. (1989) Solubility of amorphous calcium carbonate. *J. Cryst. Growth* **98**, 504–510.

Busenberg E. and Plummer L. N. (1985) Kinetic and thermodynamic factors controlling the distribution of SO_3^{2-} and Na^+ in calcites and selected aragonites. *Geochim. Cosmochim. Acta* **49**, 713–725.

Charlton S. R. and Parkhurst D. L. (2011) Modules based on the geochemical model PHREEQC for use in scripting and programming languages. *Comput. Geosci.* **37**, 1653–1663.

Chou L., Garrels R. M. and Wollast R. (1989) Kinetic Geochemistry Comparative study of the kinetics and mechanisms of dissolution of carbonate minerals. *Chem. Geol.* **78**, 269–282.

de Nooijer L. J., Toyofuku T. and Kitazato H. (2009a) Foraminifera promote calcification by elevating their intracellular pH. *Proc. Natl. Acad. Sci.* **106**, 15374–15378.

de Nooijer L. J., Langer G., Nehrke G. and Bijma J. (2009b) Physiological controls on seawater uptake and calcification in the benthic foraminifer *Ammonia tepida*. *Biogeosciences* **6**, 2669–2675.

de Nooijer L. J., Spero H. J., Erez J., Bijma J. and Reichart G. J. (2014) Biomineralization in perforate foraminifera. *Earth-Sci. Rev.* **135**, 48–58.

DePaolo D. J. (2011) Surface kinetic model for isotopic and trace element fractionation during precipitation of calcite from aqueous solutions. *Geochim. Cosmochim. Acta* **75**, 1039–1056.

Devriendt L. S., Watkins J. M. and McGregor H. V. (2017a) Oxygen isotope fractionation in the CaCO3-DIC-H2O system. *Geochim. Cosmochim. Acta* **214**, 115–142.

Devriendt L. S., McGregor H. V. and Chivas A. R. (2017b) Ostracod calcite records the $^{18}O/^{16}O$ ratio of the bicarbonate and carbonate ions in water. *Geochim. Cosmochim. Acta* **214**, 30–50.

Dissard D., Nehrke G., Reichart G.-J. and Bijma J. (2010) Impact of seawater pCO2 on calcification and Mg/Ca and Sr/Ca ratios in benthic foraminifera calcite: results from culturing experiments with *Ammonia tepida*. *Biogeosciences* **7**, 81–93.

DOE (1994) *Handbook of methods for the analysis of the various parameters of the carbon dioxide system in seawater; version 2.* ORNL/CDIAC.

Duenas-Bohorquez A., da Rocha R. E., Kuroyanagi A., Bijma J. and Reichart G. J. (2009) Effect of salinity and seawater calcite saturation state on Mg and Sr incorporation in cultured planktonic foraminifera. *Mar. Micropaleontol.* **73**, 178–189.

Elderfield H. and Ganssen G. (2000) Past temperature and δ18O of surface ocean waters inferred from foraminiferal Mg/Ca ratios. *Nature* **405**, 442–445.

Erez J. (2003) The source of ions for biomineralization in foraminifera and their implications for paleoceanographic proxies. *Rev. Mineral. Geochem.* **54**, 115–149.

Fehrenbacher J. S., Russell A. D., Davis C. V., Gagnon A. C., Spero H. J., Cliff J. B., Zhu Z. and Martin P. (2017) Link between light-triggered Mg-banding and chamber formation in the planktic foraminifera *Neogloboquadrina dutertrei*. *Nat. Commun.* **8**, 15441.

Füger A., Konrad F., Leis A., Dietzel M. and Mavromatis V. (2019) Effect of growth rate and pH on lithium incorporation in calcite. *Geochim. Cosmochim. Acta* **248**, 14–24.

Furla P., Galgani I., Durand I. and Allemand D. (2000) Sources and mechanisms of inorganic carbon transport for coral calcification and photosynthesis. *J. Exp. Biol.* **203**, 3445–3457.

Gabitov R., Sadekov A., Yapaskurt V., Borrelli C., Bychkov A., Sabourin K. and Perez-Huerta A. (2019) Elemental uptake by calcite slowly grown from seawater solution: an in-situ study via depth profiling. *Front. Earth Sci.* **7**, 51.

Geerken E., de Nooijer L. J., van Dijk I. and Reichart G. J. (2018) Impact of salinity on element incorporation in two benthic foraminiferal species with contrasting magnesium contents. *Biogeosciences* **15**, 2205–2218.

Geerken E., de Nooijer L. J., Roepert A., Polerecky L., King H. E. and Reichart G. J. (2019) Element banding and organic linings within chamber walls of two benthic foraminifera. *Sci. Rep.* **9**, 1–15.

Goetschl K. E., Purgstaller B., Dietzel M. and Mavromatis V. (2019) Effect of sulfate on magnesium incorporation in low-magnesium calcite. *Geochim. Cosmochim. Acta* **265**, 505–519.

Gothmann A. M., Stolarski J., Adkins J. F., Schoene B., Dennis K. J., Schrag D. P., Mazur M. and Bender M. L. (2015) Fossil corals as an archive of secular variations in seawater chemistry since the Mesozoic. *Geochim. Cosmochim. Acta* **160**, 188–208.

Hauzer H., Evans D., Müller W., Rosenthal Y. and Erez J. (2018) Calibration of Na partitioning in the calcitic foraminifer *Operculina ammonoides* under variable Ca concentration: Toward reconstructing past seawater composition. *Earth Planet. Sci. Lett.* **497**, 80–91.

Ishikawa M. and Ichikuni M. (1984) Uptake of sodium and potassium by calcite. *Chem. Geol.* **42**, 137–146.

Jacobson R. L. and Langmuir D. (1974) Dissociation constants of calcite and $CaHCO_3^+$ from 0 to 50°C. *Geochim. Cosmochim. Acta* **38**, 301–318.

Jacob D., Wirth R., Agbaje O., Branson O. and Eggins S. (2017) Planktic foraminifera form their shells via metastable carbonate phases. *Nat. Commun.* **8**, 1265.

Kaczmarek K., Nehrke G., Misra S., Bijma J. and Elderfield H. (2016) Investigating the effects of growth rate and temperature on the B/Ca ratio and δ11B during inorganic calcite formation. *Chem. Geol.* **421**, 81–92.

Kisakurek B., Eisenhauer A., Böhm F., Garbe-Schönberg D. and Erez J. (2008) Controls on shell Mg/Ca and Sr/Ca in cultured planktonic foraminiferan *Globigerinoides ruber*, (white). *Earth Planet. Sci. Lett.* **273**, 260–269.

Kitano Y., Okumura M. and Idogaki M. (1975) Incorporation of sodium, chloride and sulfate with calcium carbonate. *Geochem. J.* **9**, 75–84.

Lea D. W., Mashiotta T. A. and Spero H. J. (1999) Controls on magnesium and strontium uptake in planktonic foraminifera determined by live culturing. *Geochim. Cosmochim. Acta* **63**, 2369–2379.

Lippmann F. (1980) Phase diagrams depicting aqueous solubility of binary mineral systems. *Neues Jahrb. Mineral. Abh.* **139**, 1–25.

Lopez O., Zuddas P. and Faivre D. (2009) The influence of temperature and seawater composition on calcite crystal growth mechanisms and kinetics: Implications for Mg incorporation in calcite lattice. *Geochim. Cosmochim. Acta* **73**, 337–347.

Lorens R. B. and Bender M. L. (1980) The impact of solution chemistry on Mytilis edulis calcite and aragonite. *Geochimica Cosmochimica Acta* **44**, 1265–1278.

McIntire W. L. (1963) Trace element partition coefficients – a review of theory and applications to geology. *Geochim. Cosmochim. Acta* **27**, 1209–1264.

Mezger E. M., Nooijer L. J., Boer W., Brummer G. J. A. and Reichart G. J. (2016) Salinity controls on Na incorporation in Red Sea planktonic foraminifera. *Paleoceanography* **31**.

Mezger E. M., Nooijer L. J., Siccha M., Kucera M. and Reichart G.-J. (2018) Taphonomic and ontogenetic effects on Na/Ca and Mg/Ca in spinose planktonic foraminifera from the Red Sea. *Geochem. Geophys. Geosyst.* **19**, 4174–4194.

Mezger E. M., de Nooijer L. J., Bertlich J., Bijma J., Nürnberg D. and Reichart G. J. (2019) Planktonic foraminiferal spine versus shell carbonate Na incorporation in relation to salinity. *Biogeosciences* **2018**, 1–28.

de Moura Neves B., Edinger E., Hayes V. W., Devine B., Wheeland L. and Layne G. (2018) Size metrics, longevity, and growth rates in Umbellula encrinus (Cnidaria: Pennatulacea) from the eastern Canadian Arctic.. *Arctic Science* **4**, 722–749.

Mucci A. and Morse J. W. (1983) The incorporation of Mg^{2+} and Sr^{2+} into calcite overgrowths: influences of growth rate and solution composition. *Geochim. Cosmochim. Acta* **47**, 217–233.

Nehrke G., Reichart G. J., Van Cappellen P., Meile C. and Bijma J. (2007) Dependence of calcite growth rate and Sr partitioning on solution stoichiometry: Non-Kossel crystal growth. *Geochim. Cosmochim. Acta* **71**, 2240–2249.

Nehrke G., Keul N., Langer G., de Nooijer L. J., Bijma J. and Meibom A. (2013) A new model for biomineralization and trace-element signatures of Foraminifera tests. *Biogeosciences* **10**, 6759–6767.

Nürnberg D., Bijma J. and Hemleben C. (1996) Assessing the reliability of magnesium in foraminiferal calcite as a proxy for water mass temperatures. *Geochim. Cosmochim. Acta* **60**, 803–814.

Okai T., Suzuki A., Kawahata H., Terashima S. and Imai N. (2002) Preparation of a New Geological Survey of Japan Geochemical Reference Material: Coral JCp-1. *Geostand. Geoanal. Res.* **26**, 95–99.

Okumura M. and Kitano Y. (1986) Coprecipitation of alkali metal ions with calcium carbonate. *Geochim. Cosmochim. Acta* **50**, 49–58.

Politi Y., Arad T., Klein E., Weiner S. and Addadi L. (2004) Sea urchin spine calcite forms via a transient amorphous calcium carbonate phase. *Science* **306**, 1161–1164.

Ruiz-Agudo E., Kowacz M., Putnis C. V. and Putnis A. (2010) The role of background electrolytes on the kinetics and mechanism of calcite dissolution. *Geochim. Cosmochim. Acta* **74**, 1256–1267.

Spero H. J., Eggins S. M., Russell A. D., Vetter L., Kilburn M. R. and Hönisch B. (2015) Timing and mechanism for intratest Mg/Ca variability in a living planktic foraminifer. *Earth Planet. Sci. Lett.* **409**, 32–42.

Tang J., Dietzel M., Böhm F., Köhler S. J. and Eisenhauer A. (2008) Sr^{2+}/Ca^{2+} and $^{44}Ca/^{40}Ca$ fractionation during inorganic calcite formation: II. Ca isotopes. *Geochim. Cosmochim. Acta* **72**, 3733–3745.

Tesoriero A. J. and Pankow J. F. (1996) Solid solution partitioning of Sr^{2+}, Ba^{2+}, and Cd^{2+} to calcite. *Geochim. Cosmochim. Acta* **60**, 1053–1063.

Toyofuku T., Matsuo M. Y., de Nooijer L. J., Nagai Y., Kawada S., Fujita K., Reichart G.-J., Nomaki H., Tsuchiya M. and Sakaguchi H. (2017) Proton pumping accompanies calcification in foraminifera. *Nat. Commun.* **8**, 14145.

Watkins J. M., Nielsen L. C., Ryerson F. J. and DePaolo D. J. (2013) The influence of kinetics on the oxygen isotope composition of calcium carbonate. *Earth Planet. Sci. Lett.* **375**, 349–360.

Watkins J. M., Hunt J. D., Ryerson F. J. and DePaolo D. J. (2014) The influence of temperature, pH, and growth rate on the ^{18}O composition of inorganically precipitated calcite. *Earth Planet. Sci. Lett.* **404**, 332–343.

Watson E. B. (2004) A conceptual model for near-surface kinetic controls on the trace-element and stable-isotope composition of abiogenic calcite crystals. *Geochim. Cosmochim. Acta* **68**, 1473–1488.

White A. F. (1977) Sodium and potassium coprecipitation in aragonite. *Geochim. Cosmochim. Acta* **41**, 613–625.

White A. F. (1978) Sodium coprecipitation in calcite and dolomite. *Chem. Geol.* **23**, 65–72.

Wit J. C., De Nooijer L., Wolthers M. and Reichart G.-J. (2013) A novel salinity proxy based on Na incorporation into foraminiferal calcite. *Biogeosciences* **10**, 6375–6387.

Wolthers M., Nehrke G., Gustafsson J. P. and Van Cappellen P. (2012) Calcite growth kinetics: Modeling the effect of solution stoichiometry. *Geochim. Cosmochim. Acta* **77**, 121–134.

Yoshimura T., Tamenori Y., Suzuki A., Kawahata H., Iwasaki N., Hasegawa H., Nguyen L. T., Kuroyanagi A., Yamazaki T., Kuroda J. and Ohkouchi N. (2017) Altervalent substitution of sodium for calcium in biogenic calcite and aragonite. *Geochim. Cosmochim. Acta* **202**, 21–38.

Zeebe Richard (2012) History of Seawater Carbonate Chemistry, Atmospheric CO_2, and Ocean Acidification. *Annual review of earth and planetary sciences* **40**, 141–165.

Zhou X., Rosenthal Y., Haynes L., Si W., Evans D., Huang K.-F., Hönisch B. and Erez J. (in press) Planktic foraminiferal Na/Ca: A potential proxy for seawater calcium concentration. *Geochim. Cosmochim. Acta* (in press).

Associate editor: Nicholas Tosca